Cerebral Cortex, October 2015;25: 3758–3778

doi: 10.1093/cercor/bhu253
Advance Access Publication Date: 19 October 2014
ORIGINAL ARTICLE

ORIGINAL ARTICLE

NFIX Regulates Proliferation and Migration Within the Murine SVZ Neurogenic Niche

Yee Hsieh Evelyn Heng[1], Bo Zhou[5], Lachlan Harris[1], Tracey Harvey[1], Aaron Smith[1], Elise Horne[1], Ben Martynoga[4], Jimena Andersen[4], Angeliki Achimastou[4], Kathleen Cato[1], Linda J. Richards[1,2], Richard M. Gronostajski[5], Giles S. Yeo[6], François Guillemot[4], Timothy L. Bailey[3], and Michael Piper[1,2]

[1]The School of Biomedical Sciences, [2]Queensland Brain Institute, [3]Institute for Molecular Bioscience, The University of Queensland, Brisbane, QLD 4072, Australia, [4]Division of Molecular Neurobiology, MRC-National Institute for Medical Research, London NW7 1AA, UK, [5]Department of Biochemistry, Programs in Neuroscience and Genetics, Genomics & Bioinformatics, Developmental Genomics Group, New York State Center of Excellence in Bioinformatics and Life Sciences, State University of New York at Buffalo, Buffalo, NY 14203, USA, and [6]MRC Metabolic Diseases Unit, University of Cambridge Metabolic Research Laboratories, Wellcome Trust-MRC Institute of Metabolic Science, Addenbrooke's Hospital, Cambridge CB2 0QQ, UK

Address correspondence to Michael Piper, The School of Biomedical Sciences and the Queensland Brain Institute, The University of Queensland, Brisbane 4072, Australia. Email: m.piper@uq.edu.au

Abstract

Transcription factors of the nuclear factor one (NFI) family play a pivotal role in the development of the nervous system. One member, NFIX, regulates the development of the neocortex, hippocampus, and cerebellum. Postnatal *Nfix*$^{-/-}$ mice also display abnormalities within the subventricular zone (SVZ) lining the lateral ventricles, a region of the brain comprising a neurogenic niche that provides ongoing neurogenesis throughout life. Specifically, *Nfix*$^{-/-}$ mice exhibit more PAX6-expressing progenitor cells within the SVZ. However, the mechanism underlying the development of this phenotype remains undefined. Here, we reveal that NFIX contributes to multiple facets of SVZ development. Postnatal *Nfix*$^{-/-}$ mice exhibit increased levels of proliferation within the SVZ, both in vivo and in vitro as assessed by a neurosphere assay. Furthermore, we show that the migration of SVZ-derived neuroblasts to the olfactory bulb is impaired, and that the olfactory bulbs of postnatal *Nfix*$^{-/-}$ mice are smaller. We also demonstrate that gliogenesis within the rostral migratory stream is delayed in the absence of *Nfix*, and reveal that *Gdnf* (glial-derived neurotrophic factor), a known attractant for SVZ-derived neuroblasts, is a target for transcriptional activation by NFIX. Collectively, these findings suggest that NFIX regulates both proliferation and migration during the development of the SVZ neurogenic niche.

Key words: neuroblast, nuclear factor one X, olfactory bulb, rostral migratory stream, subventricular zone

Introduction

The subventricular zone (SVZ) is one of the 2 neurogenic niches in the rodent brain that continuously generates neurons throughout adult life (Kriegstein and Alvarez-Buylla 2009). Within the SVZ, the division of neural stem cells produces transit-amplifying cells, and ultimately neuroblasts. These SVZ-derived neuroblasts migrate away from the SVZ anteriorly along a distinct pathway known as the rostral migratory stream (RMS) to the olfactory bulb. Here, they differentiate into interneurons that migrate radially within the olfactory bulb to either the granule cell layer or the glomerular layer (Sun et al. 2010). Neurogenesis within the SVZ has been linked to innate olfactory responses, with deficits in SVZ neurogenesis in rodent models leading to altered behavior when confronted with a predator-specific odor, and sex-specific deficits in fertility and nurturing (females) and aggression and sexual behavior (males) (Sakamoto et al. 2011).

Neural stem cells within the SVZ are derived from the neuroepithelial progenitor cells of the embryonic forebrain, the radial glia. Indeed, fate-mapping experiments in mice have demonstrated that all parts of the telencephalic neuroepithelium, including the lateral ganglionic eminence, cortex and medial ganglionic eminence, contribute to the adult SVZ progenitor pool (Merkle et al. 2004; Young et al. 2007). Moreover, this heterogeneity is reflected in their neuronal progeny. For example, descendants of radial glia within the embryonic cortex and lateral ganglionic eminence are responsible for generating tyrosine hydroxylase-expressing and calretinin-expressing interneurons within the olfactory bulb (Whitman and Greer 2009). Interestingly, many of the genes shown to regulate radial glial self-renewal and neuronal specification and differentiation have also been shown to be functionally important within the SVZ neurogenic niche, including *Hes1* (Imayoshi et al. 2010), *Ngn2* (Brill et al. 2009), *NeuroD1* (Gao et al. 2009), *Pax6* (Brill et al. 2008), *Tbr2* (Roybon et al. 2009) and *Sox2* (Andreu-Agullo et al. 2012). However, despite these advances, our understanding of the molecular hierarchy controlling SVZ neurogenesis remains incomplete.

The migration of SVZ-derived neuroblasts to the olfactory bulb is also critical for neuronal replacement within this structure. Many cell-autonomous and non-cell-autonomous factors have been shown to control neuroblast migration. For instance, cytoskeletal factors such as doublecortin (DCX) and nude neurodevelopment protein 1-like 1 are critical cell-intrinsic proteins that are required for the migration of neuroblasts (Gleeson et al. 1999; Hippenmeyer et al. 2010). Moreover, extrinsic guidance cues such as slit and netrin are expressed within the forebrain and olfactory bulb and are required to shape the trajectory of migration through the RMS (Murase and Horwitz 2002; Nguyen-Ba-Charvet et al. 2004). Neuroblasts also migrate through a specialized glial substrate called the glial tube, which develops postnatally (Bovetti et al. 2007). The migration of neuroblasts through this astrocytic tube is facilitated by chemoattractants, including glial-derived neurotrophic factor (GDNF; Paratcha et al. 2006), but again, the molecular determinants regulating the development of this specialized substrate remain poorly understood.

The transcription factor nuclear factor one X (NFIX) has previously been implicated in regulating radial glial proliferation and differentiation within the embryonic forebrain, and the migration of neurons within the postnatal cerebellum (Piper et al. 2011; Heng et al. 2014). Here we reveal that NFIX also plays an important role in regulating these processes within the postnatal SVZ/RMS. Through the analysis of postnatal *Nfix*$^{-/-}$ mice, we demonstrate abnormal development of the SVZ and RMS in the absence of this transcription factor. Specifically, *Nfix*$^{-/-}$ mice exhibit increased numbers of neural progenitor cells within the SVZ, a finding supported by the increased numbers of spheres formed by *Nfix*$^{-/-}$ SVZ tissue in vitro in a neurosphere assay. Despite the increased levels of SVZ proliferation, the olfactory bulbs of *Nfix*$^{-/-}$ mice are smaller, with reduced numbers of interneurons expressing PAX6, calbindin and calretinin. Birthdating experiments further reveal deficits in the migration of SVZ-derived neuroblasts to the olfactory bulb. Finally, we demonstrate that gliogenesis within the RMS is delayed and identify *Gdnf* as a target for transcriptional activation by NFIX. Thus, NFIX regulates both proliferation and migration within the postnatal mouse SVZ/RMS.

Materials and Methods

Mouse Strains

Wild-type and *Nfix*$^{-/-}$ littermate mice were used in this study. These mice were maintained on a C57Bl/6J background. Timed-pregnant females were obtained by placing *Nfix*$^{+/-}$ male and *Nfix*$^{+/-}$ female mice together overnight. The following day was designated as embryonic day (E) 0 if the female had a vaginal plug. Mice were genotyped by polymerase chain reaction (PCR; Campbell et al. 2008). Transgenic mice expressing green fluorescent protein (GFP) under control of the glutamic acid decarboxylase 67 (*Gad67*) promoter were also used (Tamamaki et al. 2003), as were mice expressing GFP under the control of the *Dcx* promoter (Walker et al. 2007). The former mice have GFP knocked into the *Gad67* locus, and expression of GFP has previously been shown to colocalize with GAD67 expression (Tamamaki et al. 2003). The latter strain (*Dcx*-GFP/bacterial artificial chromosome [BAC]) was originally obtained from the Mutant Mouse Regional Resource Center and the Gene Expression Nervous System Atlas BAC transgenic project. The pattern of GFP expression in these animals matches previously reported expression of DCX (Gleeson et al. 1999). Finally, we used another BAC transgenic line expressing GFP under the control of the *Hes5* promoter. These mice have been shown previously to express GFP in neural stem cells within the adult brain (Jhaveri et al. 2010). All animals were bred at The University of Queensland under approval from the Institutional Animal Ethics Committee, and were performed according to the Australian Code of Practice for the Care and Use of Animals for Scientific Purposes.

Hematoxylin Staining

Brains from wild-type or *Nfix*$^{-/-}$ mice were dissected from the skull, blocked in 3% noble agar (Difco), and sectioned coronally at 50 μm on a vibratome (Leica). Sections were mounted and stained with Mayer's hematoxylin using standard protocols.

Immunohistochemistry

Embryos, postnatal pups and adult mice were transcardially perfused with 0.9% saline, followed by 4% paraformaldehyde, and postfixed in 4% paraformaldehyde at 4 °C. Brains were removed and sectioned at 50 μm using a vibratome. Immunohistochemistry (IHC) using the chromogen 3,3′-diaminobenzidine (DAB) was performed as described previously (Piper et al. 2009). Biotin-conjugated goat anti-rabbit IgG (BA-1000, Vector Laboratories) and biotin-conjugated donkey anti-mouse IgG (715-065-150, Jackson Immunoresearch) secondary antibodies were used at 1/1000. To perform co-immunofluorescence (IF) labeling, sections were incubated overnight with the primary antibodies at 4 °C.

They were then washed and incubated in a solution containing the secondary antibodies, before being washed again and counterstained with 4′,6-diami-dino-2-phenylindole (DAPI). The secondary antibodies used in this study were goat anti-rabbit IgG AlexaFluor 594 and goat anti-mouse IgG AlexaFluor 488 (both 1/1000; Invitrogen). Sections were then mounted in 50% glycerol diluted in phosphate-buffered saline.

For all immunohistochemical and IF analyses, at least 5 brains were analyzed. Sections labeled with DAB were imaged using an upright microscope (Zeiss upright Axio-Imager Z1) fitted with an Axio-Cam HRc camera. Sections labeled with fluorescent antibodies were imaged with a confocal microscope (Zeiss LSM 510 META) using Zen software (Zeiss). The confocal images presented are 2 μm optical sections of the labeled tissue.

Antibody Parameters

Primary antibodies used for IHC and IF on floating sections were anti-NFIX (ab101341, rabbit polyclonal, 1/10 000 IHC, 1/50 IF, Abcam), anti-GFAP (Z0334, rabbit polyclonal, 1/15 000 IHC, Dako), anti-GFAP (MAB 360, mouse monoclonal, 1/100 IF, Millipore), anti-PAX6 (AB2237, rabbit polyclonal, 1 : 20 000 IHC, Millipore), anti-GFAP (131-17719, Invitrogen, chicken polyclonal, 1/600), anti-GFAP (ab4674, chicken polyclonal, 1/200 IF, Abcam), anti-phosphohistone H3 (PHH3; 06-570, rabbit polyclonal, 1/10 000 IHC, Millipore), anti-polysialylated-neural cell adhesion molecule (PSA-NCAM) (5A5, 1/500 IHC, Developmental Studies Hybridoma Bank), anti-calbindin (CB-38a, rabbit polyclonal, 1/50 000 IHC, SWANT); anti-calretinin (CR 7699/3H, rabbit polyclonal, 1/50 000 IHC, SWANT), anti-cleaved caspase 3 (9661, rabbit polyclonal, 1/5000 IHC, Cell Signaling Technology), anti-DCX (ab18723, 1/50 000 IHC, Abcam), anti-DCX (sc8066, goat polyclonal, 1/50 IF, Santa Cruz), anti-TBR2 (rabbit polyclonal, 1/10 000 IHC, 1/250 IF, a gift from Dr Robert Hevner, University of Washington, Seattle), anti-5-bromo-2′-deoxyuridine (BrdU; G3G4, mouse monoclonal, 1/5000 IHC, Developmental Studies Hybridoma Bank), anti-Ki67 (NCL-Ki67p, rabbit polyclonal, 1/200 IF, Novocastra), anti-Ki67 (550609, mouse monoclonal, 1/200 IF, BD Pharmingen), anti-Tuj1 (MAB1195, mouse monoclonal, 1/1000 IF, R&D Systems), anti-S100β (ab66028, mouse monoclonal, 1/200 IF, Abcam), anti-MASH1 (ab74065, rabbit polyclonal, 1/10 000 IHC, Abcam), anti-SOX2 (#2784, rabbit polyclonal, 1/200 IF, Cell Signaling Technology) and anti-SOX10 (SC-17342, goat polyclonal, 1/200 IF, Santa Cruz).

Quantification of SVZ Size and Cell Numbers

To measure the area of the SVZ and RMS in postnatal wild-type and *Nfix*$^{-/-}$ brains, coronal sections at equivalent rostro-caudal positions were either immunostained or hematoxylin-stained, and imaged with an upright microscope coupled to AxioVision software (Zeiss). The cross-sectional area of the SVZ, rostral SVZ, and RMS in both wild-type and knockout samples was then calculated. Similarly, to quantify the number of CC3-, PHH3-, MASH1, TBR2, SOX2, and BrdU-positive cells within the SVZ of postnatal day 10 (P10) wild-type and knockout mice, sections were immunolabeled with the respective antibodies, then imaged. The total number of immunopositive cells within the SVZ was counted and is presented here as immunopositive cells per unit area of the SVZ. To quantify proliferating neuroblasts within the SVZ of P20 wild-type and knockout sections, IF staining of the markers DCX and Ki67 was performed. Nuclei were also labeled with DAPI. Sections were then imaged using a confocal microscope at the level of the SVZ. For each frame, the total number of DCX-positive cells was quantified, as was the number of cells positive for both DCX and Ki67. Data are presented as the number of cells expressing both DCX and Ki67 as a proportion of the total number of cells expressing DCX. To quantify interneuron populations within the olfactory bulb, P20 wild-type and knockout olfactory bulbs were sectioned coronally on a vibratome, and immunostaining was used to identify interneurons expressing PAX6, calbindin or calretinin. Sections were then imaged and the number of immunopositive cells per 100 μm within the glomerular layer and granule cell layer was counted, using representative sections from lateral, medial, dorsal and ventral regions of the respective olfactory bulbs. In all cases, at least 5 wild-type and 5 knockout brains were used for quantification. Quantification was performed blind to the genotype of the sample, and statistical analyses were performed using a two-tailed unpaired *t*-test. Error bars represent the standard error of the mean.

In Situ Hybridization

P20 brains were collected and fixed as described above ($n = 5$ for both wild-type and knockout). In situ hybridization was performed using anti-sense probes as previously described (Piper et al. 2009) with minor modifications. The hybridization temperature was 70 °C. The color reaction solution was BM Purple (Roche). In situ probes were kindly provided by Dr Jane Johnson (*Mash1*; University of Texas, Dallas, TX, USA) and by Dr Ryoichiro Kageyama (*Hes1* and *Hes5*; Kyoto University, Kyoto, Japan).

In Vivo BrdU Incorporation Assay

P8 wild-type and *Nfix*$^{-/-}$ mice were injected intraperitoneally with BrdU (Invitrogen) at 100 mg/kg. After 5 days, the animals were transcardially perfused with 0.9% saline, followed by 4% paraformaldehyde, and then postfixed in 4% paraformaldehyde at 4°C. Brains were removed and sectioned coronally at 50 μm using a vibratome. Antigen retrieval was performed by incubating sections in 2 N HCl for 45 min. IHC was then performed as described above. To quantify BrdU-positive cells in the SVZ, RMS, and ependymal cell layer of the olfactory bulb, sections at equivalent rostro-caudal positions were imaged, and the total number of BrdU-positive cells in a 200 μm^2 region was counted for both wild-type and mutant mice. To quantify BrdU-positive cells in the glomerular layer of the olfactory bulb, the number of immunopositive cells per 200 μm within the glomerular layer was counted, using representative sections from lateral, medial, dorsal and ventral regions of the respective olfactory bulbs. In all cases, at least 5 wild-type and 5 knockout brains were used for quantification. Quantification was performed blind to the genotype of the sample, and statistical analyses were performed using a two-tailed unpaired *t*-test. Error bars represent the standard error of the mean.

Microarray Analysis

To collect SVZ/RMS tissue, brains of P20 littermate wild-type ($n = 3$) and *Nfix*$^{-/-}$ mice ($n = 3$) were dissected from the skull, the SVZ exposed by cutting the brains coronally at the level of the corpus callosum, and the SVZ/RMS isolated by pinching it out with a pair of fine forceps. Total RNA was extracted using a QIAGEN RNA isolation kit, and the microarray analysis was performed at the Australian Research Council Special Research Centre for Functional and Applied Genomics (The University of Queensland, Australia) as described previously (Piper et al. 2010). Labeled and amplified material (1.5 μg/sample) was hybridized to Illumina's MouseWG-6 v2.0 Expression BeadChip at 55 °C for 18 h according

to the Illumina BeadStation 500X™ protocol. Arrays were washed and then stained with 1 μg/mL of cyanine3-streptavidin (Amersham Biosciences). The Illumina BeadArray™ reader was used to scan the arrays according to the manufacturer's instructions. Samples were initially evaluated using the BeadStudio™ software from Illumina. Quality control reports were satisfactory for all samples. The raw data were then imported into GeneSpring GX v7.3 (Agilent). Data were initially filtered using GeneSpring normalization algorithms. Quality control data filtering was then performed using the Bead detection score *P*-value, and with expression values below background, as determined by the cross-gene error model. Differential expression was determined by the one-way ANOVA-Welch's approximate *t*-test without a multiple testing correction. A cutoff *P*-value of 0.05 was used for the mean difference between wild-type and *Nfix*$^{-/-}$ SVZ tissue. In addition, a 1.5-fold-change filter was imposed on the genes from the ANOVA dataset. Pathway analysis was performed using Ingenuity Pathway Analysis.

Bioinformatic Promoter Screen

The NFI-binding motif was generated as reported previously (Heng et al. 2012) from published chromatin immunoprecipitation-sequencing (ChIP-seq) data for NFI (pan-NFI antibody used) (Pjanic et al. 2011). The DNA-binding domains of all NFI proteins are highly similar (Mason et al. 2009). In brief, we performed motif discovery using the MEME algorithm (Bailey et al. 2009) on ChIP-seq peaks redeclared using the ChIP-Peak algorithm (Schmid and Bucher 2010) from the published ChIP-seq "tag" data for NFI. We then identified potential NFI-binding sites by scanning the complete mouse genome downloaded from the UCSC Genome Browser (mm9, July 2007) (Fujita et al. 2011) using the MEME-derived motif and the FIMO motif-scanning program (Grant et al. 2011). FIMO was run on the mouse genome (without repeat masking) using a 0-order background generated on the entire mouse genome, and a pseudocount of 0.1. All potential binding sites with a *P*-value of $\leq 10^{-4}$ were reported in the region of −3000 to +200 bp relative to the transcription start site (TSS). Putative NFI-binding sites near the promoters of genes were identified by viewing the FIMO output using the UCSC genome browser.

Neurosphere Assay

Brains of P15 wild-type and *Nfix*$^{-/-}$ mice were isolated from the skull and dissected manually on the coronal plane to expose the lateral ventricles at the level of the corpus callosum. The SVZ was carefully removed using forceps, then cut into fine pieces before enzymatic digestion was performed by incubation in 0.05% trypsin at 37 °C for 15 min, a process that culminated in a single cell suspension. After centrifugation at 110 × g for 5 min, cells were carefully dissociated and resuspended in 5 mL of pre-warmed neurosphere medium containing 20 ng/mL of epidermal growth factor (EGF), 10 ng/mL of basic fibroblast growth factor (bFGF) and 3.5 μg/mL of heparin. The cell suspension was then run through a 50 μm filter. The primary tissue was plated at a concentration of 2.5×10^5 cells in 5 mL of medium in a T-25 flask for 7 days. The total number of spheres that had formed was counted after 7 days. The neurospheres were then dissociated and passaged at a constant density of 2.5×10^5 cells in 5 mL of medium and then counted 7 days later. This was then repeated for another 4 more passages. Sphere diameter was also measured at each passage, and the data shown represent the combined results from all the passages.

Neuroblast Migration Assay

To evaluate the contribution of NFIX during neuroblast migration, neurospheres from passage 4 wild-type and *Nfix*$^{-/-}$ cohorts were seeded onto coverslips coated with poly-L-ornithine (10 mg/mL) and placed into a 6-well plates containing DMEM- F12 (with 5% fetal bovine serum and 1% penicillin and streptomycin). Spheres of approximately equal sizes (100–200 μm in diameter) were used for this assay. Spheres were cultured for 3 days at 37 °C. A set of spheres from either genotype were also cultured with bath-applied recombinant GDNF (120 ng/mL; R&D Systems, recombinant human GDNF) for the 3 days. Following this adherent neurospheres were fixed with 4% PFA, and DCX expression was analyzed using IF staining with an anti-DCX antibody (1 : 1000, Abcam, AB18723) and a fluorescent secondary antibody (AlexaFluor 488; 1/500). Cell nuclei were stained with DAPI. Cultures were imaged using a fluorescence microscope (Zeiss upright Axio-Imager Z1). The distance each DCX-positive cell had migrated from the edge of the adherent sphere was measured with ImageJ. Spheres isolated from $n = 5$ wild-type and $n = 5$ *Nfix*$^{-/-}$ mice were counted. Quantification was performed blind to the genotype of the sample, and statistical analyses were performed using a two-tailed unpaired *t*-test. Error bars represent the standard error of the mean.

Luciferase Assay

Our bioinformatic promoter screen identified 2 potential NFI-binding sites within the *Gdnf* promoter, at +44 bp relative to the TSS (chromosome 15: 7811055–7811069, GTGGCCCGAATCCCA) and at −5 bp relative to the TSS (chromosome 15: 7811006–7811020, CTGGGCGGGGCCCCG). The constructs used in the luciferase assay were full-length *Nfix*, *Nfia* and *Nfib* expression constructs (each in the vector pCAGIG-IRES-GFP) and a *Renilla* luciferase construct containing 575 bp of the upstream promoter region of the mouse *Gdnf* gene (*Gdnf* Prom: chromosome 15: 7810505–7811080). This luciferase construct was obtained from Switchgear Genomics. A truncated *Gdnf* promoter construct was also generated, which lacked the 2 putative NFI-binding sites. This construct contained 470 bp of the upstream promoter region of the mouse *Gdnf* gene (chromosome 15: 7810505–7810975). DNA was transfected into Neuro2A cells using FuGene (Invitrogen). *Cypridina* luciferase was added to each transfection as a normalization control. After 48 h, luciferase activity was measured using a dual luciferase system (Switchgear Genomics). Within each experiment, each treatment was replicated 6 times. Each experiment was also independently replicated a minimum of 3 times. The pCAGIG vector alone did not significantly alter *Gdnf* promoter-driven luciferase activity (data not shown). Statistical analyses were performed using an ANOVA. Error bars indicate the standard error of the mean.

Electrophoretic Mobility Shift Assay

Nuclear extracts were isolated from the cortex of E18 brains, and from COS cells overexpressing HA-tagged versions of either NFIX or an unrelated control transcription factor, AP2. Electrophoretic mobility shift assays (EMSAs) were performed using radiolabeled annealed oligonucleotides containing *Gdnf* consensus sites from our bioinformatics screen. EMSA reactions were carried out as described previously using 1 μg of nuclear extract (Piper et al. 2010). Oligonucleotide sequences were: *Gdnf* −5, 5′- CCGGGACCTTCTGG GCGGGGCCCCGCGCTCC -3′ (upper strand), 5′- CCGGGGAGCGCGG GGCCCCGCCCAGAAGGTC -3′ (lower strand); *Gdnf* +44, 5′- CCGGGCT

GGATGGGATTCGGGCCACTTGGAC -3′ (upper strand), 5′- CCGG GTCCAAGTGGCCCGAATCCCATCCAGC -3′ (lower strand).

Supershift assays were performed with an anti-HA antibody (Sigma; #H9658).

Reverse Transcription and Quantitative Real-time PCR

SVZ/RMS and olfactory bulb tissue from P20 wild-type and *Nfix*$^{-/-}$ mice were microdissected and immediately snap-frozen. Total RNA was extracted using a RNeasy Micro Kit (Qiagen). Reverse transcription was performed using Superscript III (Invitrogen) and qPCR was performed as described previously (Piper et al. 2010). Briefly, 0.5 µg total RNA was reverse-transcribed with random hexamers. qPCRs were carried out in a Rotor-Gene 3000 (Corbett Life Science) using the SYBR Green PCR Master Mix (Invitrogen). All the samples were diluted 1/100 with RNase/DNase free water and 5 µL of these dilutions were used for each SYBR Green PCR containing 10 µL of SYBR Green PCR Master Mix, 10 µM of each primer, and deionized water. The reactions were incubated for 10 min at 95 °C followed by 40 cycles with 15 s denaturation at 95 °C, 20 s annealing at 60 °C, and 30 s extension at 72 °C. The primer sequences used in this study can be found in Table 1.

qPCR Data Expression and Analysis

After completion of the PCR amplification, the data were analyzed with the Rotor-Gene software as described previously (Piper et al. 2009). When quantifying the mRNA expression levels, the housekeeping gene *glyceraldehyde 3-phosphate dehydrogenase* (*Gapdh*) was used as a relative standard. All the samples were tested in triplicate. For all qPCR analyses, RNA from 8 biological replicates for both wild-type and *Nfix*$^{-/-}$ mice were interrogated. Relative transcript levels were assessed using the $\Delta\Delta C_t$ method as described previously (Piper et al. 2014). Statistical analyses were performed using a two-tailed unpaired *t*-test. Error bars represent the standard error of the mean.

Results

NFIX Is Expressed Within the SVZ and RMS of Postnatal and Adult Mice

We showed previously that the transcription factor NFIX is expressed within the developing forebrain, with expression evident within the ventricular zone of the neocortex and hippocampus. Furthermore, NFIX is expressed within the adult neurogenic niches of the brain, including the SVZ (Campbell et al. 2008). However, the expression of NFIX within specific cell types of the SVZ, RMS and olfactory bulb has not been defined in detail. To address this, we analyzed NFIX expression in postnatal and adult mice using IHC. The specificity of the anti-NFIX antibody we used

Table 1 Primer sequences used in this study

Gene	Sequence
Gapdh For	GCACAGTCAAGGCCGAGAAT
Gapdh Rev	GCCTTCTCCATGGTGGTGAA
Gdnf For	TGAAGACCACTCCCTCGG
Gdnf Rev	GCTTGTTTATCTGGTGACCTTTTC
Dcx For	TGGAAGCATGGATGAACTGG
Dcx Rev	CATGTTGGCAGATGTCTTTACG
Pax6 For	CTCCTAGTCACATTCCTATCAGC
Pax6 Rev	GCAAAGCACTGTACGTGTTG
Gfap For	AGTGGTATCGGTCTAAGTTTG
Gfap Rev	CGATAGTCGTTAGCTTCGTG

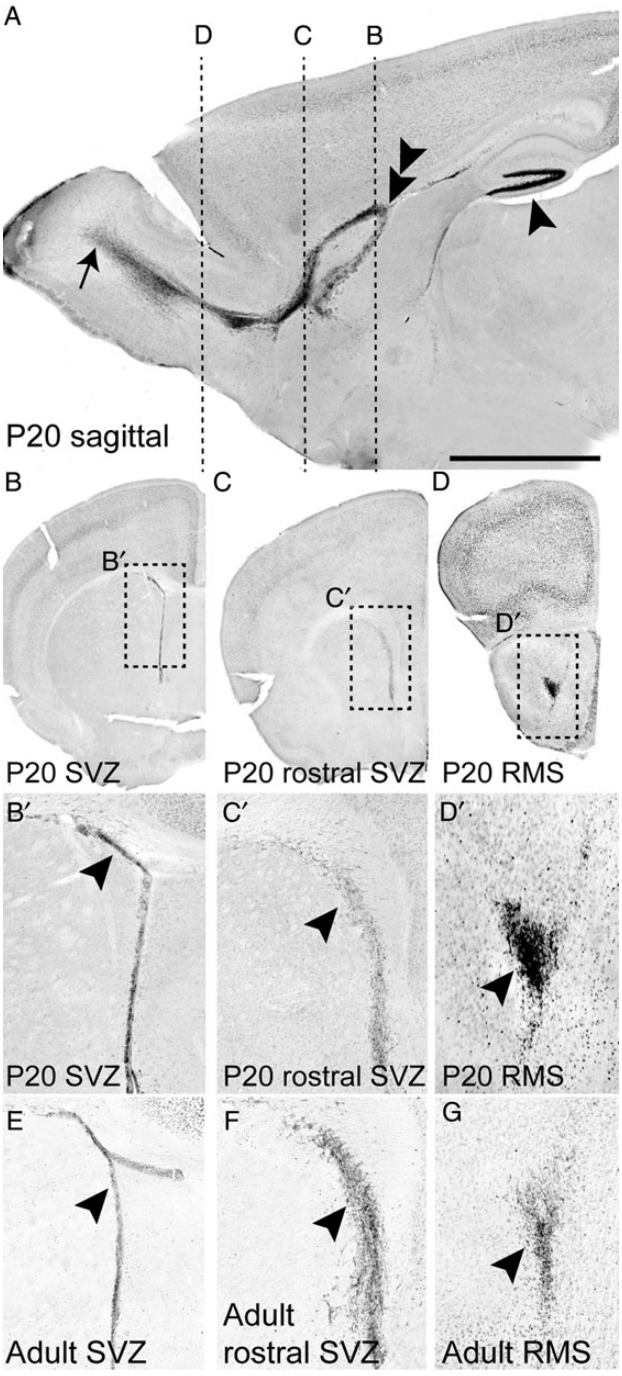

Figure 1. NFIX is expressed within the postnatal and adult SVZ. Expression of NFIX in sagittal (*A*) and coronal (*B*–*G*) sections of P20 (*A*–*D*) and adult (*E*–*G*) mice. (*A*) At P20, NFIX expression was observed within the hippocampus (arrowhead), the SVZ (double arrowhead) and olfactory bulb (arrow). The dotted lines in *A* indicate the rostro-caudal position from which panels (*B*–*D*) are taken. At the level of the corpus callosum, NFIX expression was evident within the SVZ (*B*, arrowhead in *B*′). Similarly, within the rostral SVZ (*C*, arrowhead in *C*′) and RMS (*D*, arrowhead in *D*′), NFIX expression was clearly seen. Within the adult brain, NFIX expression was also observed within the SVZ (arrowheads in *E*,*F*) and RMS (arrowhead in *G*). Scale bar (in *A*): *A*–*D*, 600 µm; *B*′–*D*′ and *E*–*G*, 150 µm.

has been previously demonstrated (Harris et al. 2013); moreover, we observed no specific staining within the olfactory bulb of P20 *Nfix*$^{-/-}$ mice (Supplementary Fig. 1*A*,*B*). In wild-type mice, NFIX expression was observed within the germinal ventricular zone at E18 (Supplementary Fig. 1*C*,*D*). NFIX expression was also detected within the emerging SVZ and RMS at P5 and P10 (data not shown). By P20, the expression of NFIX within the SVZ and RMS was clearly seen in both sagittal and coronal sections from wild-type mice (Fig. 1*A*–*D*). Expression of NFIX was also observed in the olfactory bulb and the hippocampus (Fig. 1*A*). Using co-IF labeling, coupled with confocal microscopy, on the SVZ from P12 mice, we investigated the cell type-specific expression of NFIX within this developing postnatal neurogenic niche. At this age, nearly all neural stem cells (defined as cells expressing GFAP, but not s100β) were immunopositive for NFIX (Table 2). Similarly, proliferating progenitor cells in this niche (Ki67 +ve, DCX –ve; encompassing dividing stem cells and transit-amplifying cells), ependymal cells (cells immediately adjacent to the lateral ventricle expressing both GFAP and s100β), and neuroblasts (DCX +ve cells) were predominantly immunopositive for NFIX (Table 2). Interestingly, at this age, SVZ astrocytes (defined as cells not adjacent to the lateral ventricle that expressed GFAP and s100β) and cells of the oligodendrocyte lineage (SOX10 +ve) did not express NFIX. These findings demonstrate that NFIX is expressed by neural progenitor cells, transit-amplifying cells and neuroblasts within the postnatal SVZ neurogenic niche.

In the adult brain, NFIX expression was also clearly evident within the SVZ and RMS (Fig. 1*E*–*G*). To determine cell type-specific expression of NFIX within the adult SVZ and RMS, we again used co-IF labeling and confocal microscopy. First, we analyzed the expression of NFIX within the SVZ of a strain of mice expressing GFP under the control of the neural stem cell-specific *Hes*5 promoter. Co-labeling of the SVZ of adult *Hes*5-GFP mice with antibodies against another neural stem cell marker, GFAP, and NFIX, revealed that cells expressing both *Hes*5-GFP and GFAP also expressed NFIX (Fig. 2*A*–*E*). Interestingly, many cells were immunopositive for NFIX, but not for GFP. Some of these cells are likely to be ependymal cells, as s100β-expressing ependymal cells lining the lateral ventricles were also immunopositive for NFIX (Fig. 2*F*–*I*).

Within the SVZ and RMS, migrating neuroblasts express the microtubule-associated protein DCX, and GAD67, one of the principal enzymes used during the production of the inhibitory neurotransmitter γ-aminobutyric acid (GABA). To determine whether neuroblasts within the adult brain express NFIX, we analyzed the expression of this transcription factor in a strain of mice expressing GFP under the control of the DCX promoter (*Dcx*-GFP). GFP-expressing neuroblasts within the SVZ and RMS were seen to express NFIX (Supplementary Fig. 2*A*–*H*). Similarly,

Table 2 Cell type-specific of NFIX expression within the postnatal SVZ

Marker expression	Cellular population	Number of population expressing NFIX
GFAP +ve; s100β –ve	Neural progenitor cell	289/290
GFAP +ve; s100β +ve	Mature astrocyte	0/35
GFAP +ve; s100β +ve (adjacent to the LV)	Ependymal cell	115/115
Ki67 +ve; DCX –ve	Proliferating cell (neural progenitor cells and transit-amplifying cells)	112/112
Ki67 +ve; DCX +ve	Dividing neuroblast	64/64
Ki67 –ve; DCX +ve	Non-dividing neuroblast	77/100
SOX10 +ve	Oligodendrocytes and oligodendrocyte precursor cells	0/48

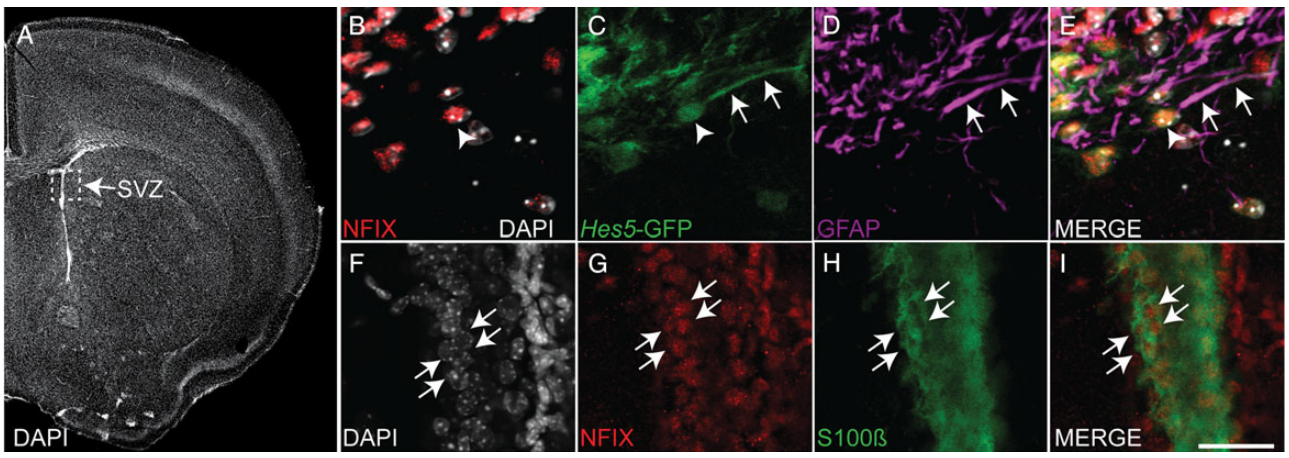

Figure 2. Neural progenitor cells and ependymal cells express NFIX within the adult SVZ. Coronal sections through the SVZ of adult wild-type (*A*, *F*–*I*) and *Hes*5-GFP (*B*–*E*) mice. (*A*) A low power image of a representative section labeled with DAPI. The boxed region indicates the approximate location within the SVZ from which the higher magnification images of other sections were obtained. Co-IF labeling and confocal microscopy were used to determine the cell type-specific expression of NFIX within the adult SVZ. Cell nuclei were labeled with DAPI (white). Within the SVZ of *Hes*5-GFP mice, GFP-positive neural stem cells (green, *C*) co-expressed GFAP (magenta) and NFIX (red). The neural stem cell indicated demonstrates the expression of GFP and NFIX within the nucleus (arrowheads in *B* and*E*), as well as colocalization of GFP and GFAP within the cytoplasm (arrows in *D* and *E*). Within the SVZ of wild-type mice (*F*), ependymal cells (arrows *F*–*I*) express s100β (green, *H* and *I*) and NFIX (red; *G* and *I*). Scale bar (in *I*); 300 μm for *A*; 25 μm for *B*–*I*.

Gad67-GFP-expressing neuroblasts within the RMS (Tamamaki et al. 2003) also co-expressed NFIX (Supplementary Fig. 2*I–L*). However, although all neuroblasts within the RMS expressed NFIX, there were also cells surrounding the RMS that were immunoreactive for NFIX, but not for GFP (Supplementary Fig. 2*H*,*L*). These cells could be RMS astrocytes, which comprise the glial tube through which SVZ-derived neuroblasts migrate en route to the olfactory bulb (Peretto et al. 1997). Co-IF labeling with anti-GFAP antibodies supported this hypothesis, with confocal microscopic analyses revealing that there were some cells

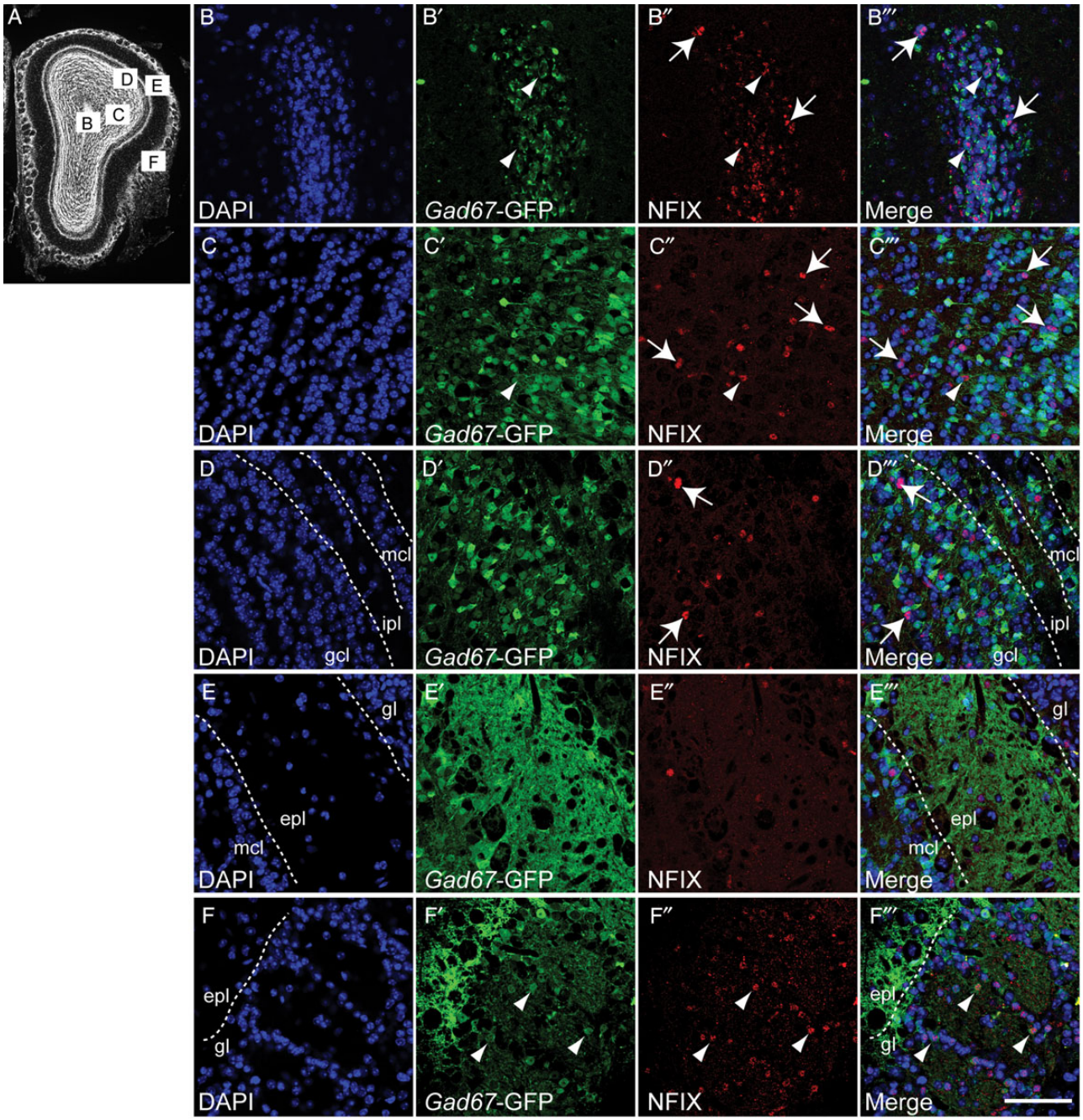

Figure 3. Cell type-specific expression of NFIX within the olfactory bulb of adult *Gad67*-GFP mice. Coronal sections through the olfactory bulb of adult *Gad67*-GFP mice. (*A*) A low power image of a representative olfactory bulb section labeled with DAPI. The boxed regions indicate the location within the olfactory bulb from which the higher magnification images were obtained. Co-IF labeling and confocal microscopy were used to determine the cell type-specific expression of NFIX (red) within the adult olfactory bulb. Cell nuclei were labeled with DAPI (blue). (*B*) Within the core of the olfactory bulb, expression of NFIX coincided with that of GFP within neuroblasts (arrowheads, *B′–B‴*). However, there were also some cells present that were immunoreactive for NFIX, but not for GFP (arrows, *B″–B‴*). (*C*) Within the granule cell layer (gcl), there were scattered NFIX-expressing cells, but these were mostly GFP-negative (arrows, *C″–C‴*), although we did locate a small number of cells expressing both GFP and NFIX (arrowheads, *C′–C‴*). (*D*) Similarly, we observed scattered NFIX-expressing cells within the internal plexiform layer (ipl) and mitral cell layer (mcl) (arrows in *D″–D‴*), but these cells did not express GFP. (*E*) Within the external plexiform layer, we saw very few NFIX-expressing cells, and these cells did not express GFP. (*F*) Within the glomerular layer (gl), we observed numerous GFP-expressing cells that were also immunoreactive for NFIX (arrowheads in *F′–F‴*). Scale bar (in *F‴*); 250 μm for *A*; 40 μm for remaining panels.

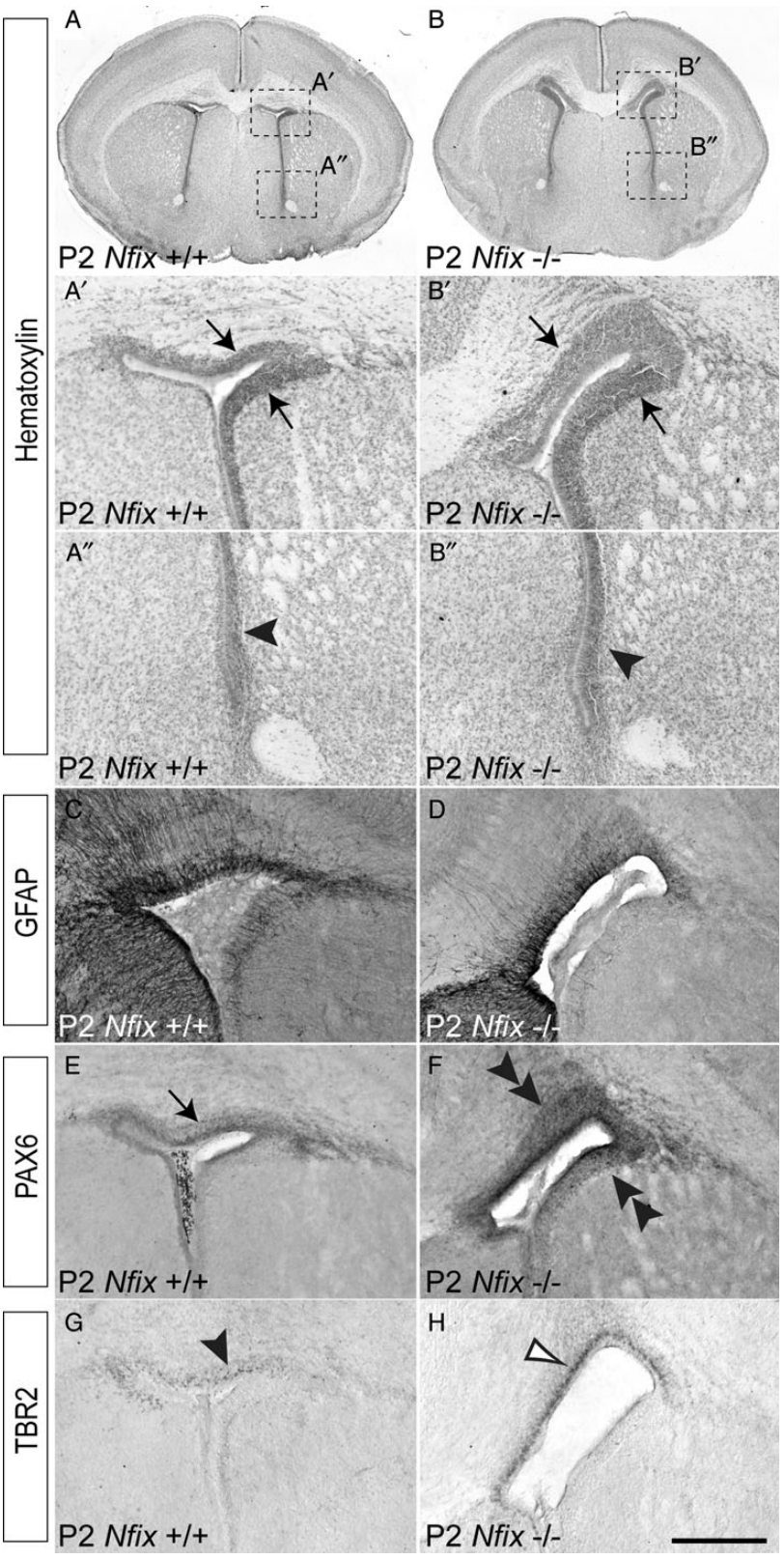

Figure 4. Deficits in SVZ structure within the early postnatal period of *Nfix*$^{-/-}$ mice. Coronal sections of P2 *Nfix*$^{+/+}$ (*A*, *C*, *E* and *G*) and *Nfix*$^{-/-}$ (*B*, *D*, *F* and *H*) mice at the level of the corpus callosum. Hematoxylin staining of wild-type and *Nfix*$^{-/-}$ sections revealed that the SVZ of mutant mice had become thickened by this age compared with the wild type. Higher magnification views of the dorsal (*A*′ and *B*′) and ventral (*A*″ and *B*″) lateral ventricles indicated that the dorsolateral SVZ of the mutant was thickened in comparison with the control (compare arrows in *A*′ and *B*′), whereas the ventral SVZ appeared normal (compare arrowheads in *A*″ and *B*″). Expression of GFAP at the cortical midline of the mutant (*D*) was still markedly lower than that seen in the control (*C*). Interestingly, there were more cells expressing PAX6 in the mutant (double arrowheads in *F*) than in the control (arrow in *E*). Similarly, TBR2 expression within the SVZ was elevated in *Nfix*$^{-/-}$ mice (compare open arrowhead in *H* with the arrowhead in *G*). Scale bar (in *H*): 600 μm for *A* and *B*; 150 μm for *A*′, *A*″, *B*′, *B*″ and *C*–*H*.

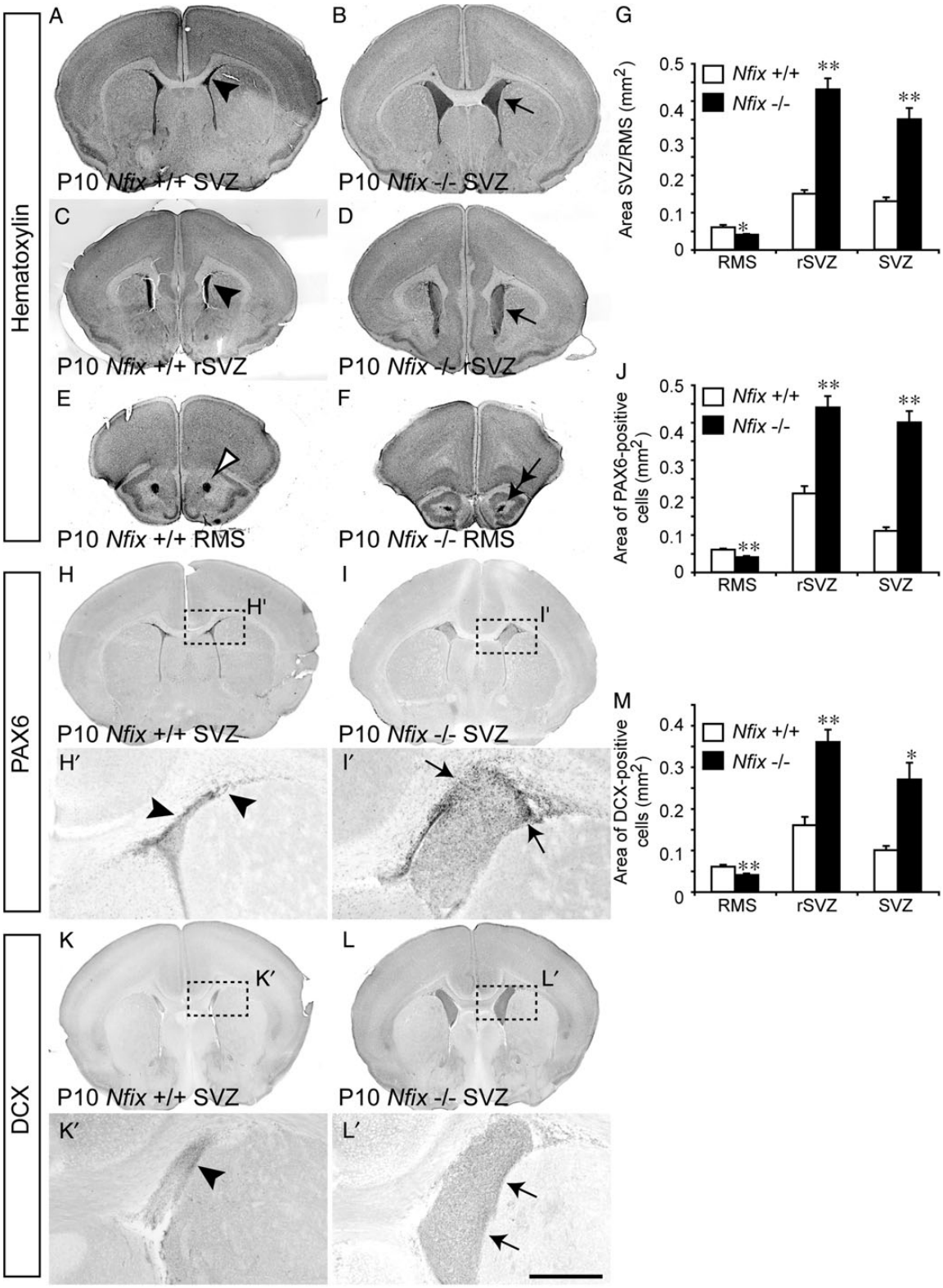

Figure 5. Expansion of the SVZ in mice lacking *Nfix*. Coronal sections of P10 *Nfix*$^{+/+}$ (*A*, *C*, *E*, *H* and *K*) and *Nfix*$^{-/-}$ (*B*, *D*, *F*, *I*, *L*) mice at the level of the corpus callosum (*A*, *B*, *H*, *I*, *K*, *L*), rostral SVZ (rSVZ—immediately rostral to the corpus callosum; *C* and *D*) and RMS (*E* and *F*). Hematoxylin staining revealed a dramatically expanded SVZ within the mutant mice (arrows in *B* and *D*) compared with controls (arrowheads *A* and *C*). The cross-sectional area of the RMS, however, was reduced in the mutant (compare the open arrowhead in *E* with the double-headed arrow in *F*). *G* represents quantification of the cross-sectional area of the SVZ in the mutant, which was significantly larger, and the RMS, which was significantly reduced, relative to the wild-type controls. Expression of the stem cell marker PAX6 (*H*, *H*′, *I* and *I*′) and the neuroblast marker DCX (*K*, *K*′, *L* and *L*′) also revealed markedly more cells expressing these factors within the SVZ of *Nfix*$^{-/-}$ mice than in comparison with the controls (compare arrowheads in *H*′ and *K*′ with the arrows in *I*′ and *L*′), whereas the RMS within the mutant was smaller (*J* and *M*). $^{*}P < 0.05$, $^{**}P < 0.01$, *t*-test. Scale bar (in *L*′): 600 μm.

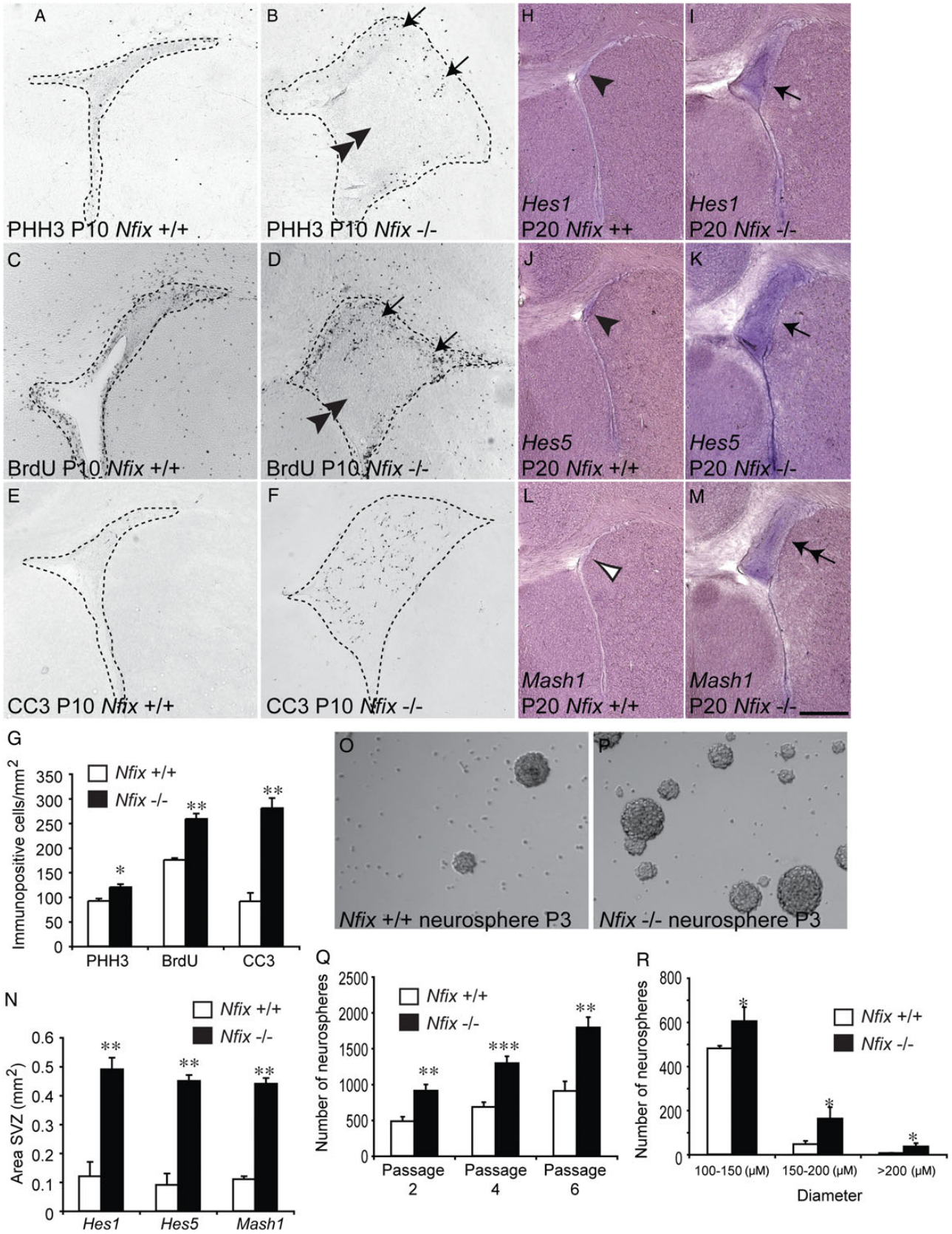

Figure 6. Increased proliferation within the SVZ of postnatal *Nfix*$^{-/-}$ mice. Coronal sections at the level of the corpus callosum through P10 (*A–F*) and P20 (*H–M*) *Nfix*$^{+/+}$ (*A*, *C*, *E*, *H*, *J* and *L*) and *Nfix*$^{-/-}$ (*B*,*D*, *F*, *I*, *K* and *M*) mice. There were significantly more PHH3-positive, BrdU-positive (BrdU administered 2 h prior to sacrifice), and cleaved caspase 3-positive (CC3) cells per unit area of the mutant SVZ than the wild-type (*A–G*). Interestingly, with both PHH3 and BrdU labeling in the mutant, the proliferative cells were observed on the periphery of the SVZ (arrows in *B* and *D*), but to a lesser extent in the center of the SVZ (double arrowheads, *B* and *D*). At P20, expression of the neural stem

expressing both GFAP and NFIX along the periphery of the RMS (Supplementary Fig. 2M–P). Collectively, these findings indicate that NFIX is expressed by multiple cellular populations within the adult SVZ and RMS.

Expression of NFIX Within the Developing and Adult Olfactory Bulb

Given that NFIX is expressed within the olfactory bulb at P20 (Fig. 1A), we examined NFIX expression within this structure in more detail. NFIX was not expressed within the olfactory bulb of embryonic or early postnatal mice (data not shown). At P10, expression of NFIX became apparent, with weak expression within the subependymal layer; these cells are likely to be SVZ-derived neuroblasts (Supplementary Fig. 3A). Low expression of NFIX was also detected within cells within the laminae of the olfactory bulb, including cells within the glomerular layer and the granule cell layer (Supplementary Fig. 3B). By P20, NFIX was strongly expressed within the olfactory bulb, particularly by cells within the subependymal layer and the glomerular layer, but also by scattered cells within the other laminae of the olfactory bulb (Supplementary Fig. 3C,D). This expression pattern was maintained within the adult olfactory bulb (Supplementary Fig. 3E,F). Within the adult olfactory bulb, we used the *Gad67*-GFP line to assess cell type-specific expression of NFIX. These analyses revealed that *Gad67*-GFP-expressing neuroblasts within the subependymal layer and periglomerular interneurons express NFIX within the adult olfactory bulb (Fig. 3). Moreover, co-IF staining for GFAP and NFIX showed that olfactory bulb astrocytes express NFIX (Supplementary Fig. 4E–H).

Development of the SVZ Is Aberrant in Postnatal *Nfix*$^{-/-}$ Mice

The expression of NFIX in neural stem cells within the postnatal SVZ suggests a role for this transcription factor in regulating the development of this neurogenic niche. In support of this, we reported previously that P16 *Nfix*$^{-/-}$ mice exhibit more PAX6-expressing cells within the SVZ than littermate controls (Campbell et al. 2008). However, when this phenotype first becomes evident is unclear. We therefore analyzed the germinal zones around the lateral ventricles of wild-type and *Nfix*$^{-/-}$ mice at E18 (Supplementary Fig. 5A,B). Hematoxylin staining revealed an enlarged cingulate cortex in *Nfix*$^{-/-}$ mice, in line with previous reports (Campbell et al. 2008), as well as a smaller corpus callosum, and IHC further revealed reduced GFAP expression at the cortical midline (Supplementary Fig. 5G,H). We have previously reported that neural progenitor cells within the dorsal telencephalon are delayed in their differentiation in the absence of NFIX (Heng et al. 2014), and the analysis of both the radial glial marker PAX6 and the intermediate progenitor cell marker TBR2 within the germinal zones surrounding the lateral ventricles supported this finding, with more cells expressing these markers within the germinal zones of the mutant. However, this phenotype appeared subtle at the level of the corpus callosum at E18 (Supplementary Fig. 5C–F).

By P2, however, the germinal zones around the ventricles of *Nfix*$^{-/-}$ mice were appreciably different from those of wild-type littermate controls. Hematoxylin staining revealed that the region lining the lateral ventricles of *Nfix*$^{-/-}$ mice was thickened dorso-laterally, although it appeared normal ventrally (Fig. 4A, B). Expression of GFAP within the mutant at this age was still diminished, but the expression of both PAX6 and TBR2 was elevated in comparison with controls (Fig. 4C–H). This phenotype was even more pronounced at P10, where hematoxylin staining and PAX6 IHC revealed that the SVZ of *Nfix*$^{-/-}$ mice was significantly larger in area than that of controls (Fig. 5A–D,G–J). Interestingly, this situation was reversed when we analyzed the cross-sectional area of the RMS, which was significantly reduced in mice lacking *Nfix* (Fig. 5E–G). Staining with the neuroblast marker DCX supported this finding, revealing significantly more DCX +ve cells within the SVZ of mutant mice, but a reduced cross-sectional area of the RMS (Fig. 5K–M). These findings indicate that, although proliferation in the SVZ of mutant mice is likely to be increased, there are fewer cells migrating to the olfactory bulb, suggesting that migration through the RMS is impaired in these mice. This phenotype was recapitulated at P20, with increased numbers of cells expressing PAX6, DCX, and another neuroblast marker, PSA-NCAM, within the SVZ of *Nfix*$^{-/-}$ mice (Supplementary Fig. 6). These findings demonstrate that the SVZ in *Nfix*$^{-/-}$ mice begins to develop significant abnormalities in the early postnatal period, and suggest that deficits in both proliferation and neuroblast migration are responsible for the SVZ phenotype within these mice.

Elevated Proliferation Within the SVZ of Postnatal *Nfix*$^{-/-}$ Mice

To assess the contribution of NFIX to proliferation within the SVZ/RMS, we analyzed proliferation via the expression of the mitotic marker PHH3 at P10. As anticipated, there were significantly more PHH3 +ve cells per unit area in the mutant when compared with littermate controls (Fig. 6A,B,G). Similarly, labeling cells in S-phase with BrdU 2 h prior to sacrifice revealed significantly more proliferating cells within the SVZ of *Nfix*$^{-/-}$ mice (Fig. 6C,D,G). Interestingly, there were also more apoptotic cells per unit area of the mutant SVZ (Fig. 6E–G). Analysis of the expression of the Notch effector genes *Hes1* and *Hes5*, both markers for SVZ neural stem cells, by in situ hybridization further revealed elevated levels of expression of these factors within the SVZ of *Nfix*$^{-/-}$ mice. Similarly, *Mash1*, a marker for transit-amplifying cells (Kim et al. 2011), was more highly expressed within the mutant SVZ (Fig. 6H–N). Finally, cell counts performed on the SVZ of P10 wild-type and *Nfix*$^{-/-}$ mice revealed significantly more cells per unit area expressing the neural stem cell marker SOX2 (Andreu-Agullo et al. 2012) and also more transit-amplifying cells expressing MASH1 in the mutant in comparison with the control (Fig. 7A–D,G).

These findings are suggestive of increased proliferation within the SVZ of mice lacking *Nfix*. To probe this further, we isolated neural progenitor cells from the SVZ of P15 *Nfix*$^{-/-}$ and wild-type littermate mice, and cultured them in vitro for 6 passages using a

cell markers *Hes1* and *Hes5* was increased within the mutant SVZ (compare arrows in I and K with arrowheads in H and J). Similarly, the expression of *Mash1*, which labels transit-amplifying cells within the SVZ neurogenic niche, was elevated within *Nfix*$^{-/-}$ mice (compare double-headed arrow in M with open arrowhead in L). (N) Quantification revealed a significantly larger SVZ region expressing *Hes1*, *Hes5* and *Mash1* within *Nfix*$^{-/-}$ mice. (O–Q) Culturing SVZ-derived cells in an in vitro neurosphere assay resulted in significantly higher numbers of neurospheres (Q) in tissue isolated from *Nfix*$^{-/-}$ mice (P) when compared with wild-type controls (O). Neurospheres derived from *Nfix*$^{-/-}$ tissue were also significantly larger than those isolated from wild-type controls (R). Panels O and P are neurospheres from passage 3 (P3). *$P < 0.05$, **$P < 0.01$, ***$P < 0.001$ t-test. Scale bar (in M): 100 μm for A–F; 125 μm for H–M; 100 μm for O and P.

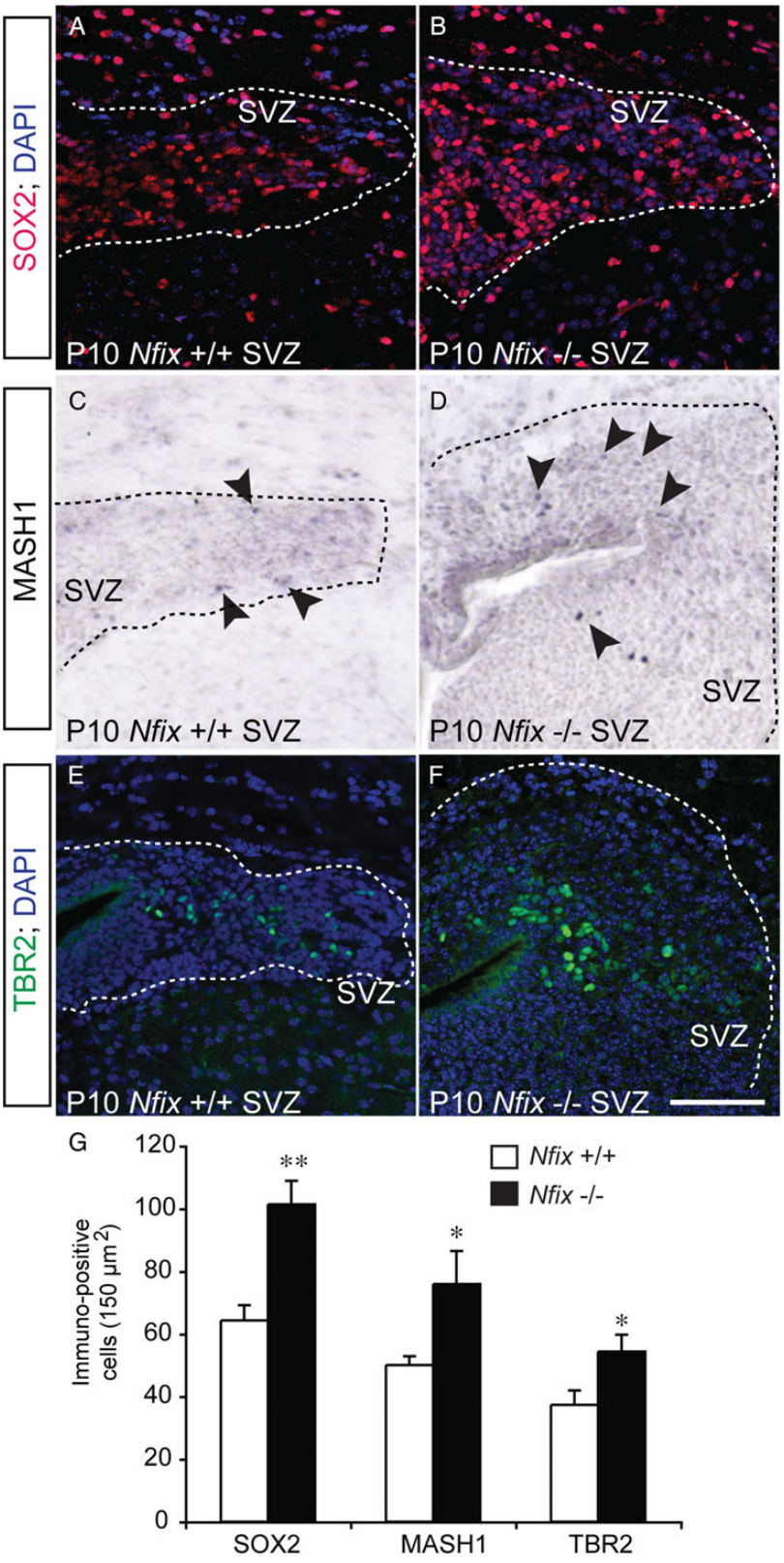

Figure 7. Increased numbers of neural stem cells and transit-amplifying cells in the SVZ of *Nfix* mutant mice. Coronal sections of P10 $Nfix^{+/+}$ and $Nfix^{-/-}$ mice revealing expression of the neural stem cell marker SOX2 (*A* and *B*), the transit-amplifying cell marker MASH1 (*C* and *D*) and of TBR2, a marker for a subpopulation of SVZ-derived neuroblasts (*E* and *F*) within the SVZ. The SVZ is delineated by the dashed lines in each image. There were significantly more cells expressing SOX2, MASH1 and TBR2 in the mutant in comparison with the control (*G*). $^{*}P < 0.05$, $^{**}P < 0.01$, *t*-test. Scale bar (in *F*): 100 μm.

neurosphere assay. This analysis revealed the presence of significantly more neurospheres at each passage in tissue isolated from *Nfix*$^{-/-}$ mice (Fig. 6O–Q). Moreover, there were significantly larger neurospheres in those cultures derived from the SVZ of *Nfix*$^{-/-}$ mice, indicative of elevated levels of proliferation. Collectively, these findings reveal that the proliferation of neural progenitor cells within the SVZ of postnatal *Nfix*$^{-/-}$ mice is elevated, suggestive of a role for this transcription factor in the repression of progenitor cell proliferation within this neurogenic niche.

Neuroblast Migration to the Olfactory Bulb Is Diminished in the Absence of NFIX

Interestingly, despite the increased levels of proliferation within the SVZ of *Nfix*$^{-/-}$ mice, both the RMS and olfactory bulbs of mutant mice were smaller than in their littermate controls (Figs 5E–G and 8A,B; Supplementary Fig. 7A–E). This, coupled with the large accumulation of neuroblasts expressing the markers DCX (Fig. 5) and TBR2 (Brill et al. 2009; Fig. 7E–G), within the SVZ of these mice, suggests that neuroblasts are unable to migrate normally through the RMS to the olfactory bulb in the absence of this transcription factor. Analysis of sagittal sections of P20 brains provided further support for this. In wild-type mice, hematoxylin-stained sections clearly revealed the trajectory of the RMS (Fig. 8A), and neuroblasts, characterized by the expression of PSA-NCAM and DCX, were readily visualized within the RMS (Fig. 8C,E). In the mutant, however, the RMS was smaller, there were fewer DCX-positive cells within the RMS, and the expression of PSA-NCAM within the RMS was almost absent (Fig. 8B,D,F).

To further investigate the migration of SVZ-derived neuroblasts, we performed a pulse-chase experiment with BrdU. *Nfix*$^{+/+}$ and *Nfix*$^{-/-}$ mice were administered an injection of BrdU (100 mg/kg) at P8, and the location of labeled cells was analyzed 5 days later at P13. In line with our previous findings relating to proliferation, we saw significantly more BrdU-positive cells per unit area of the SVZ in the mutant than in the control. However, there were significantly fewer BrdU-positive cells within the RMS and the ependymal layer and the glomerular layer of the olfactory bulb (Fig. 8G–Q), suggesting that neuroblasts derived from SVZ progenitors labeled at P8 had not migrated as far as those from the control cohort. To further investigate the migration of SVZ-derived neuroblasts, we performed a migration assay by enabling cultured neurospheres from wild-type and mutant mice to adhere to coverslips and to differentiate, through the removal of the mitogenic growth factors EGF and bFGF. Three days later, the distance migrated from parental spheres by DCX-expressing cells was quantified, revealing that wild-type neuroblasts had migrated, on average, significantly further than those from *Nfix*$^{-/-}$ mice (Fig. 9). This finding suggests that the cell-autonomous migration of SVZ-derived neuroblasts is abnormal in the absence of *Nfix*.

As they migrate from the SVZ through the RMS towards the olfactory bulb, neuroblasts proliferate, then exit the cell cycle, and stop expressing proliferative markers such as Ki67 (Smith and Luskin 1998). Our SVZ expression analysis (Table 2) had shown that all of the proliferating neuroblasts investigated, and the majority of those that were no longer proliferating, expressed NFIX. If the migration of neuroblasts was indeed impaired in *Nfix*$^{-/-}$ mice, we hypothesized that proportionally fewer DCX-expressing cells would be labeled with proliferative markers in the mutant, due to the fact that they would exit the cell cycle within the SVZ, rather than later in their migratory trajectory. In support of this, co-IF labeling of the SVZ of P20 wild-type and mutant mice with DCX and Ki67 revealed that, although there were more DCX-expressing cells within the mutant SVZ (Supplementary Fig. 6I–L), the proportion of proliferating neuroblasts was significantly smaller than that of controls (Fig. 10A–G), suggestive of the majority of these neuroblasts exiting the cell cycle within the SVZ, not within the RMS.

Reduced Interneuron Numbers in the Olfactory Bulb of *Nfix*$^{-/-}$ Mice

Given the deficits in migration of neuroblasts through the RMS within *Nfix*$^{-/-}$ mice, we investigated whether this phenotype culminated in reduced interneuron numbers within the olfactory bulb. SVZ progenitors located in different regions of the SVZ produce distinct neuronal progeny, with progenitors in the dorsal SVZ producing tyrosine hydroxylase-expressing periglomerular cells and superficial granule cells, those in the RMS and anterior SVZ generating calretinin-expressing periglomerular cells and granule cells, and those in the ventral SVZ producing calbindin-expressing periglomerular cells and deep granule cells (Young et al. 2007). PAX6 is expressed by both dopaminergic periglomerular cells and by a subpopulation of granule cells in wild-type mice (Brill et al. 2008). At P20 in the absence of *Nfix*, we observed significantly fewer PAX6-expressing cells within the glomerular and granule cell layer (Fig. 10H,K,N). Similarly, we observed significantly fewer calbindin- and calretinin-expressing cells within the glomerular layer of the mutant olfactory bulb (Fig. 10I,J,L,M,O,P). Given that the expansion in the SVZ only manifested dorsally in mutant mice, yet reductions in the numbers of multiple populations of interneurons derived from across the SVZ germinal zones were observed, these findings are illustrative of a global deficit in neuroblast migration from the SVZ to the olfactory bulb in the absence of *Nfix* and likely underlies the reduced size of the olfactory bulbs in these mutant mice.

Nfix$^{-/-}$ Mice Display Reduced Gliogenesis Within the RMS

The environmental context through which neuroblasts navigate the RMS is also critical. Glial tubes, which form in the postnatal period, form a conduit via which neuroblasts migrate through the RMS to the olfactory bulb. Given the previously described role for NFI factors in mediating gliogenesis (Brun et al. 2009; Whitman and Greer 2009; Singh, Bhardwaj, et al. 2011; Singh, Wilczynska, et al. 2011), we analyzed the expression of the glial marker, GFAP, within sagittal sections of P20 wild-type and *Nfix*$^{-/-}$ mice. In wild-type mice, GFAP-positive fibers clearly delineated the RMS (Fig. 11A). In the mutant, however, the expression of GFAP was markedly lower within the RMS and olfactory bulb (Fig. 11B), suggesting that gliogenesis is reduced within these regions of *Nfix*$^{-/-}$ mice. This finding is analogous to previous reports within the postnatal hippocampus (Heng et al. 2014), and suggests that a deficit in glial tube genesis may be the underlying mechanism responsible, at least in part, for the migratory phenotype seen in these mice.

Gdnf Is a Target for Transcriptional Activation by NFIX Within the RMS

NFIX has previously been shown to regulate gliogenesis, and the expression of glial-specific markers such as GFAP expression in vitro (Brun et al. 2009; Singh, Wilczynska, et al. 2011). To identify additional novel targets of NFIX during development of the SVZ and RMS, we performed a microarray on microdissected SVZ/RMS tissue from P20 wild-type and *Nfix*$^{-/-}$ mice. This analysis identified over 800 genes as being misregulated in the mutant,

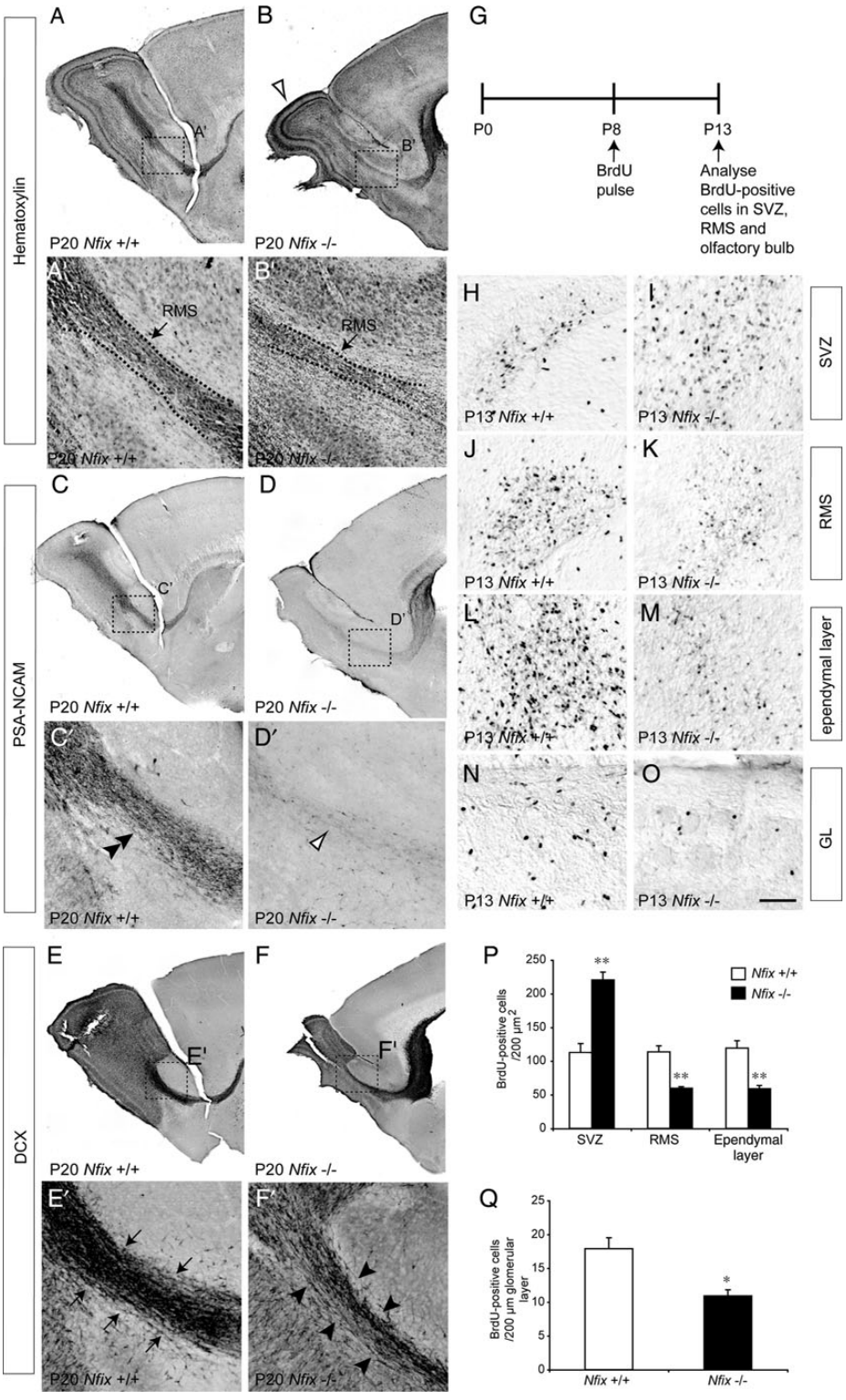

Figure 8. Abnormal migration through the RMS in postnatal mice lacking *Nfix*. (*A–F*) Sagittal sections through $Nfix^{+/+}$ (*A*, *C* and *E*) and $Nfix^{-/-}$ (*B*, *D* and *F*) mice. Hematoxylin staining of wild-type mice (*A*) revealed a well-demarcated RMS (dashed lines in *A′*). The RMS of $Nfix^{-/-}$ mice (*B*) was markedly smaller (dashed lines in *B′*), as was the olfactory bulb (open arrowhead in *B*). The expression of PSA-NCAM was also reduced within the RMS of mutant mice (compare double arrowhead in *C′* with the open arrowhead in *D′*). Similarly, expression of DCX in the wild-type RMS (*E*, arrows encompass the RMS in *E′*) was more extensive than within the mutant RMS (*F*, arrowheads encompass the RMS in *F′*). (*G*) Experimental protocol for BrdU-pulse labeling experiment. (*H–O*) Coronal sections of $Nfix^{+/+}$ and $Nfix^{-/-}$ mice at the level of the SVZ (*H* and *I*), RMS (*J* and *K*), ependymal layer of the olfactory bulb (*L* and *M*), and glomerular layer (GL) of the olfactory bulb (*N* and *O*), revealing BrdU-labeled cells. There were significantly more BrdU-labeled cells within the SVZ, but significantly fewer labeled cells within the RMS and olfactory bulb, of mutant mice in comparison with wild-type controls (*P* and *Q*). $^{*}P < 0.05$, $^{**}P < 0.01$, *t*-test. Scale bar (in *O*): 600 μm for *A–F*; 100 μm for *A′–F′*; 75 μm for *H–O*.

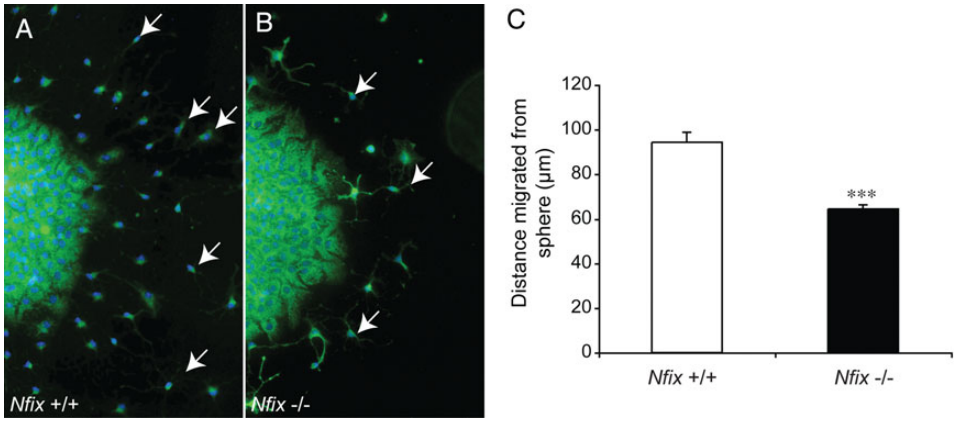

Figure 9. Reduced migration of *Nfix*$^{-/-}$ neuroblasts in vitro. Wild-type (*A*) and *Nfix*$^{-/-}$ (*B*) SVZ-derived neurospheres of similar dimensions were cultured for 72 h in the absence of mitogenic growth factors. The expression of DCX (green) was used to reveal migratory neuroblasts (arrows in *A* and *B*). (*C*) Neuroblasts isolated from the SVZ of wild-type mice migrated, on average, significantly further than those from *Nfix*$^{-/-}$ mice. Cell nuclei are labeled with DAPI (blue). ***$P < 0.005$, *t*-test. Scale bar (in *B*): 100 μm.

using a significance value of $P < 0.05$ via ANOVA and a fold-change cutoff of 1.5. Functional annotation of these transcripts using Ingenuity Pathway Analysis identified many processes as being misregulated in the mutant, including cellular development nervous system development and function, cellular movement and neurobiological disease (Supplementary Fig. 8). Key transcripts upregulated in the mutant SVZ included the progenitor cell markers *Hes1*, *Dlx1* and *Dlx2* (Fig. 11C and Table 3). We have previously demonstrated regulation of *Hes1* by NFI family members (Piper et al. 2010) and Notch signaling is critical for the maintenance of the SVZ neurogenic niche (Imayoshi et al. 2010); thus, it seems likely that the proliferative phenotype we observed in the SVZ of *Nfix*$^{-/-}$ mice (Figs 5–7) stems, at least in part, from misregulation of the Notch signaling pathway. Downregulated transcripts included the guidance receptors *Plxnd1* and *Unc5b*, as well as *Flt1*, the receptor for vascular endothelial growth factor (VEGF) (Fig. 11C and Table 4). Interestingly, *Gdnf*, which has previously been shown to promote migration through the RMS (Paratcha et al. 2006), was also downregulated in the mutant (Fig. 11C and Table 4). Validation of the array results using qPCR confirmed that levels of *Gdnf* mRNA were significantly lower in the mutant SVZ/RMS and olfactory bulb (Fig. 11*D*). In line with our immunohistochemical data, levels of *Dcx* mRNA were significantly higher in the mutant SVZ/RMS, but lower in the olfactory bulb of the mutant, and the levels of *Gfap* and *Pax6* mRNA were significantly lower in the olfactory bulb of *Nfix*$^{-/-}$ mice (Fig. 11*D*).

These array and qPCR findings suggested that diminished *Gdnf* expression within the RMS of *Nfix*$^{-/-}$ mice may underlie part of the phenotype exhibited by these mice. To determine whether *Gdnf* is a direct target for transcriptional control by NFIX, we screened the *Gdnf* promoter in silico for potential NFI-binding sites (see Materials and Methods) and identified 2 putative NFI motifs close to the *Gdnf* TSS (−5 and +44). Furthermore, NFIX was able to bind to an oligonucleotide probe containing the −5 sequence in vitro in an electrophoretic mobility shift assay (Fig. 11*E*,*F*). Finally, we used a reporter gene assay to investigate whether NFIX could activate *Gdnf* promoter-driven transcriptional activity. A fragment of the *Gdnf* promoter containing the putative NFI-binding site was able to significantly activate reporter gene expression in a luciferase assay conducted in Neuro2A cells, and this reporter gene expression was significantly increased by the co-expression of NFIX, as well as by the co-expression of the other NFI family members reported to be expressed within the adult SVZ, NFIA and NFIB (Plachez et al. 2012; Fig. 11*G*). Moreover, luciferase expression driven by a truncated version of the *Gdnf* promoter lacking the NFI-binding site was unable to be enhanced by NFIX, indicative of this site being critical for NFI-mediated activation of *Gdnf* promoter-mediated transcription. Finally, we sought to determine whether *Nfix*$^{+/+}$ and *Nfix*$^{-/-}$ neuroblasts were similarly responsive to GDNF in vitro, by culturing wild-type and mutant spheres with 120 ng/mL of bath-applied GDNF in the neuroblast migration assay (Fig. 9). Interestingly, both wild-type and mutant cells were similarly responsive to GDNF. Wild-type cells cultured in the presence of GDNF migrated 30.4% further than wild-type cells cultured without GDNF, whereas mutant cells cultured with GDNF migrated 29.3% further than mutant cells cultured without GDNF ($P < 0.05$, ANOVA). Taken together, our data suggest that NFIX is involved in the activation of *Gdnf* transcription within the olfactory bulb and RMS, and that, in the absence of *Nfix*, the reduction in *Gdnf* expression is responsible for at least part of the decreased migration of SVZ-derived neuroblasts within these mice.

Discussion

Unlike the postnatal human SVZ, in which the birth of olfactory neurons diminishes rapidly after 18 months of age (Sanai et al. 2011; Wang et al. 2011; Bergmann et al. 2012), neurogenesis within the SVZ niche continues throughout life in rodents such as mice (Alvarez-Buylla and Garcia-Verdugo 2002). The ongoing production of olfactory bulb interneurons within the postnatal and adult rodent brain relies upon both the proliferation of neural progenitor cells within the SVZ and the migration of their progeny through the RMS to the olfactory bulb, where they differentiate and mature into granule and periglomerular cells (Kriegstein and Alvarez-Buylla 2009). This intricate process relies on a host of factors, both cell-intrinsic and cell-extrinsic to the progenitor cells and neuroblasts, that must work in concert to ensure the generation of the requisite number of interneurons required for replacement within the olfactory bulb (Whitman and Greer 2009). Here, we identify the transcription factor NFIX as a vital contributor to the development of the postnatal SVZ/RMS, with abnormalities in both proliferation and migration evident within this neurogenic niche in mice lacking this gene.

Studies into the development of other regions of the brain have also highlighted a central role for NFIX in the control of neural progenitor cell proliferation and the migration of their progeny (Heng et al. 2012; Harris et al. 2014). With relation to the

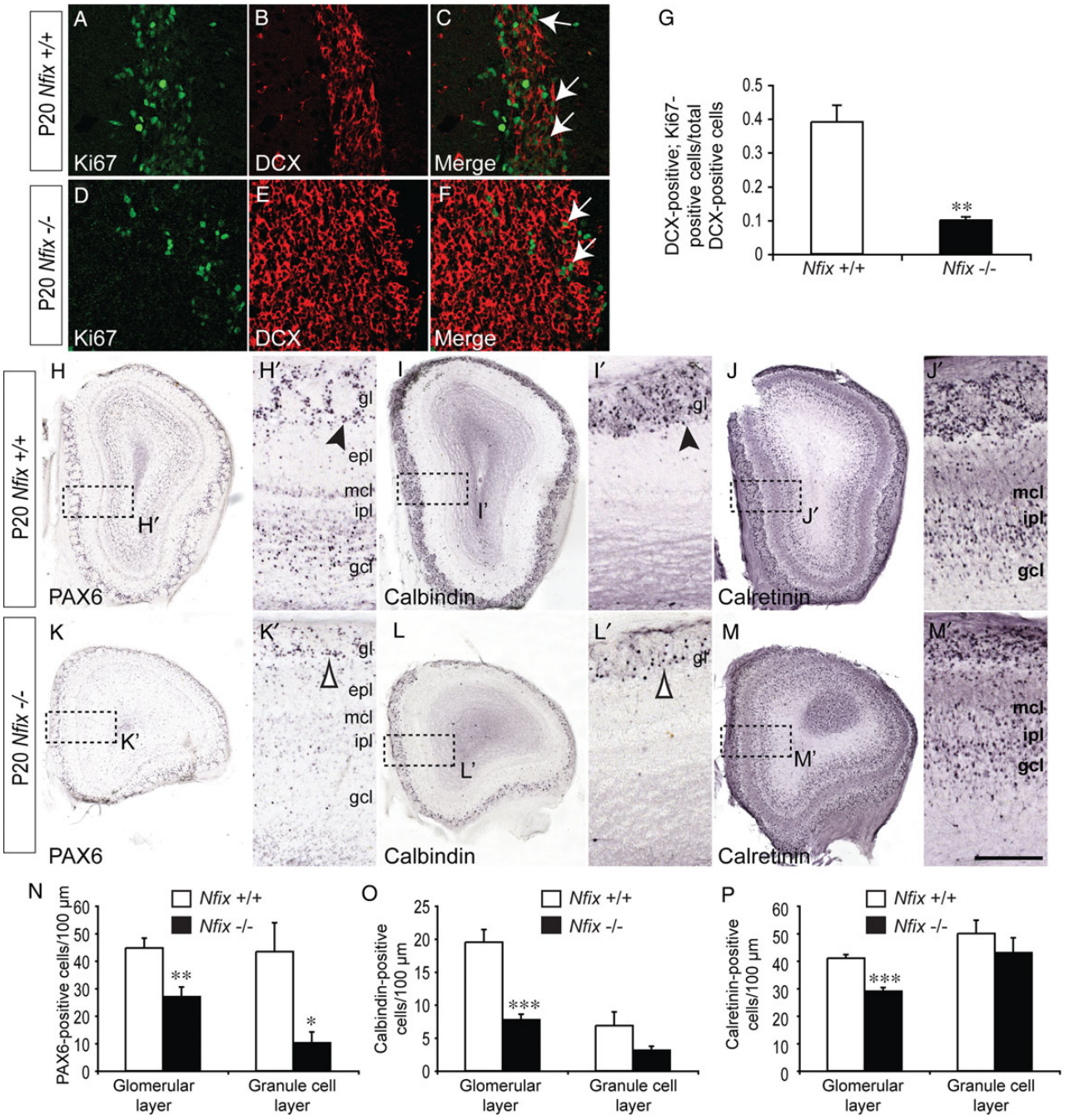

Figure 10. Decreased populations of interneurons within the olfactory bulb of *Nfix*$^{-/-}$ mice. Coronal sections through the SVZ (*A–F*) and olfactory bulb (*H–M*) of *Nfix*$^{+/+}$ and *Nfix*$^{-/-}$ mice. (*A–F*) Confocal sections through the SVZ of *Nfix*$^{+/+}$ (*A–C*) and *Nfix*$^{-/-}$ (*D–F*) mice revealing the expression of Ki67 (green) and DCX (red). Arrows in *C* and *F* indicate cells expressing both DCX and Ki67. Quantification reveals that a significantly greater proportion of DCX-positive cells in the wild-type retain Ki67 expression than within the mutant (*G*). (*H–M*) Expression of the interneuron markers PAX6 (*H* and *K*), calbindin (*I* and *L*) and calretinin (*J* and *M*) within the olfactory bulbs of *Nfix*$^{+/+}$ and *Nfix*$^{-/-}$ mice. There were significantly fewer PAX6-expressing cells within the glomerular layer (compare arrowhead in *H′* with the open arrowhead in *K′*) and granule cell layer of the mutant mice at this age (*N*). Similarly, there were fewer calbindin-expressing neurons (compare arrowhead in *I′* with the open arrowhead in *L′*) and calretinin-expressing neurons (*J* and *M*) in the mutant in comparison with the control (*O* and *P*). gl, glomerular layer; epl, external plexiform layer, mcl, mitral cell layer; ipl, internal plexiform layer; gcl, granule cell layer. *P<0.05, **P<0.01, ***P<0.001, *t*-test. Scale bar (in *M′*): 75 µm for *A–F* and *H′–M′*; 300 µm for *H–M*.

control of self-renewal and cell cycle exit, NFIX acts to promote the differentiation of neural progenitor cells within the developing neocortex and hippocampus, in part via the transcriptional repression of Sox9 (Heng et al. 2014), a factor pivotal for the induction and maintenance of cortical neural progenitors (Scott et al. 2010). Indeed, NFI transcription factors have been shown to regulate neural progenitor cell differentiation through a variety of different mechanisms, including the repression of stem cell self-renewal genes (Piper et al. 2010; Piper et al. 2014), the activation of differentiation-specific programs of gene expression (Cebolla and Vallejo 2006), and through the epigenetic control of DNA methylation (Namihira et al. 2009).

We have also recently reported a role for NFIX in the development (Heng et al. 2014) and function (Harris et al. 2013) of the

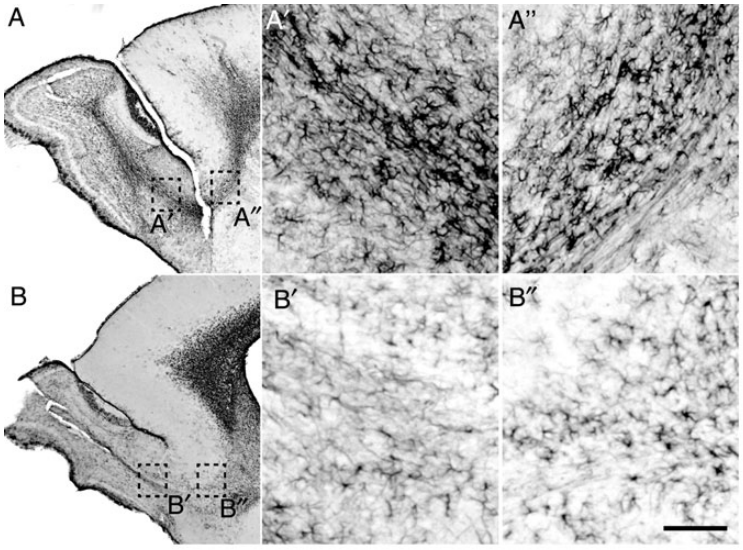

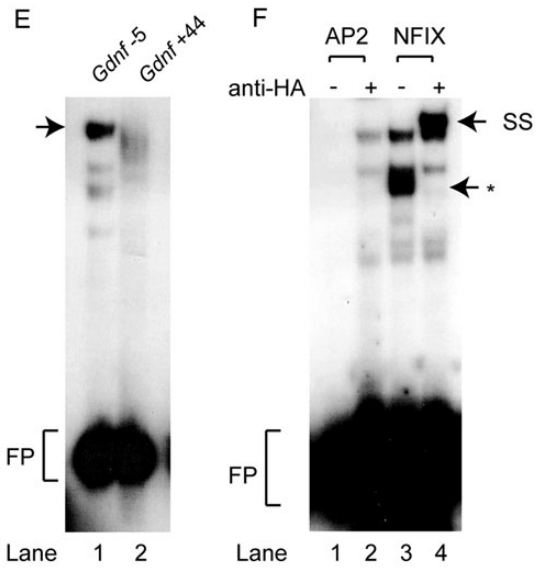

C

Downregulated	Fold change	Function
Gdnf	-2.02	Neurotrophic factor
Unc5b	-1.69	Axon guidance receptor
Flt1	-1.63	Vascular endothelial growth factor receptor
Pxnd1	-1.61	Axon guidance receptor
Upregulated	**Fold change**	**Function**
Calb	2.76	Calcium-binding protein
Dcx	2.16	Microtubule-associated protein
Hes1	1.84	Notch pathway
Th	1.82	Enzyme in dopamine biosynthetic pathway

D

Gene	Source	Relative mRNA level in control	Relative mRNA level in KO	*P* value
Gdnf	SVZ/RMS	0.8	0.55	0.03
Gdnf	OB	0.44	0.16	0.01
Dcx	SVZ/RMS	27	52.8	0.01
Dcx	OB	146	98.7	0.003
Gfap	OB	29.3	13.8	0.002
Pax6	OB	13.7	10.5	0.04

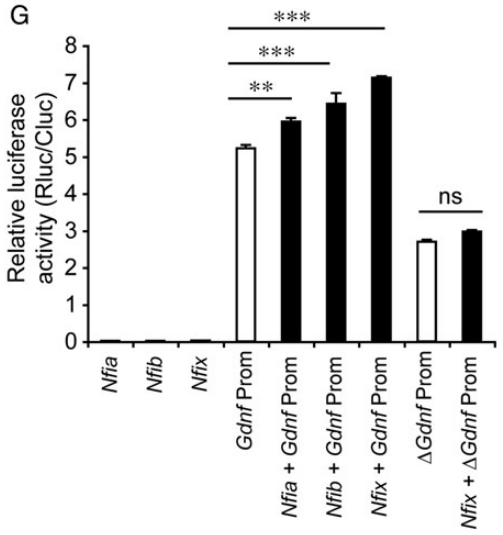

Figure 11. *Gdnf* is a direct target for transcriptional activation by NFIX. (*A* and *B*) Sagittal sections through *Nfix*$^{+/+}$ (*A*) and *Nfix*$^{-/-}$ (*B*) mice at P20. The expression of GFAP within the RMS of wild-type mice at this age is extensive (*A*′ and *A*″), but is markedly reduced in the mutant RMS (*B*′ and *B*″). (*C*) Microarray analyses revealed transcripts that were downregulated or upregulated in the SVZ/RMS of *Nfix*$^{-/-}$ mice at P20. (*D*) qPCR validation revealed that the level of *Gdnf* mRNA was significantly lower within both the SVZ/RMS and olfactory bulb (OB) of the mutant in comparison with the control at P20. Mutant mice also exhibited elevated levels of *Dcx* mRNA within the SVZ/RMS, but reduced levels of *Dcx*, *Gfap* and *Pax6* mRNAs within the olfactory bulb. (*E* and *F*) Results of EMSA. (*E*) E18 mouse cortical nuclear extracts were incubated with radiolabeled probes for the −5 (lane 1) and +44 (lane 2) consensus sites. A factor from the nuclear extract bound to the −5 probe (arrow). FP, free probe. (*F*) Nuclear extracts from COS cells expressing HA-tagged versions of the transcription factors AP2 (lanes 1 and 2) or NFIX (lanes 3 and 4) were incubated with radiolabeled probes for the −5 consensus site. There was no specific binding in the lanes containing the nuclear extracts from the AP2-expressing cells (lanes 1 and 2). A factor from the nuclear extract containing the NFIX expression construct did bind to the probe (*; lane 3). Inclusion of an anti-HA antibody into the binding reaction caused a supershift in this band (SS, lane 4). (*G*) Luciferase reporter gene assay performed in Neuro2A cells. Expression of NFIA, NFIB or NFIX elicited negligible luciferase activity, whereas transfection of a *Gdnf* promoter-driven luciferase reporter construct elicited reporter gene induction. Co-transfection of the *Nfix* expression construct and the *Gdnf* promoter resulted in a significantly increased level of luciferase activity. Similarly, co-transfection of *Nfia* or *Nfib* also significantly increased luciferase expression. However, *Nfix* was unable to enhance the activity of a truncated *Gdnf* promoter construct (Δ*Gdnf* prom) lacking the putative NFI-binding site. $^{**}P < 0.01$, $^{***}P < 0.001$, ANOVA. ns, not significant. Scale bar (in *B*″): 600 μm for *A* and *B*; 100 μm for *A*′ and *B*″.

other main neurogenic niche within the brain, the subgranular zone of the dentate gyrus, showing that NFIX mediates progenitor cell differentiation within this niche (Heng et al. 2014). Here, we extend our earlier description of the SVZ of *Nfix*$^{-/-}$ mice (Campbell et al. 2008), revealing that NFIX is also important for proliferation within the postnatal SVZ. Our studies demonstrate an increase in proliferation within the *Nfix*$^{-/-}$ postnatal SVZ, with significantly more proliferative cells in this region, as well as increased expression of progenitor cell markers including PAX6, SOX2, *Hes1* and *Hes5*, as well as MASH1, a marker for transit-amplifying cells. While it is likely that these findings reflect elevated proliferation within the SVZ, one potential caveat to this interpretation is that neuroblasts continue to proliferate within the SVZ/RMS. When considered in light of the diminished migration within these mutant mice, the attribution of the increased proliferation within the *Nfix*$^{-/-}$ SVZ solely to enhanced proliferation of

Table 3 Key examples of transcripts upregulated in the SVZ/RMS of *Nfix*$^{-/-}$ mice at P20

Functional classification (Ingenuity)	Upregulated genes
Cellular growth and proliferation	*Hes1*, *Dicer 1*, *Sox4*, *Igfbp6*, *Igfbp3*, *E2f1*, *Igfbp4*, *Socs2*, *Cntfr*
Nervous system development and function	*Map1b*, *Sfrp2*, *Grik5*, *Dlx1*, *Dlx2*, *Dcx*, *Gad1*, *Nrxn2*
Cellular function and maintenance	*Sema4A*, *Sox4*, *Mtor*, *Cebpb*, *Ifngr2*, *Sgk1*
Cancer	*Stra13*, *Flh2*, *Xpa*, *Chst8*, *Chic2*

Table 4 Key examples of transcripts downregulated in the SVZ/RMS of *Nfix*$^{-/-}$ mice at P20

Functional classification (Ingenuity)	Downregulated genes
Nervous system development and function	*Gdnf*, *Grik*, *Chat*, *Foxo1*, *Adam17*, *Gas7*, *Kcn2*, *Slc5a4*
Neurological disease	*Slit3*, *Flt1*, *Spock 3*, *Dock4*, *Kifib*, *Itgb4*, *Msx1*, *Slc5a7*, *Plxnd1*, *Scn2b*
Cell cycle	*E2f6*, *Rarres 2*, *Bcl2*, *Kit*, *Rarb*, *Gas7*
Cellular movement	*Unc5b*, *Fgf10*, *Akap9*, *Alcam*, *Gab1*, *Klf2*

neural progenitor cells becomes problematic. However, our in vitro neurosphere assay clearly demonstrated enhanced proliferation of SVZ tissue isolated from *Nfix*$^{-/-}$ mice over multiple passages. Furthermore, many of the neuroblasts within the mutant SVZ had in fact exited the cell cycle, and were no longer proliferative. Collectively, these data are strongly indicative of increased numbers of proliferating neural progenitor cells in the SVZ of mice lacking *Nfix*.

Indeed, recent reports have shown that NFIX is an important regulator of both proliferation of stem cells and of their subsequent differentiation, both within and outside the central nervous system. For example, within the hematopoietic system, NFIX was recently identified as being expressed by stem and progenitor cells, and was shown to promote their survival in vivo (Holmfeldt et al. 2013). Moreover, NFIX has been demonstrated to be instrumental for differentiation within the developing skeletal musculature, driving the switch from embryonic-specific to fetal-specific programs of gene expression (Messina et al. 2010). By what means then, does NFIX regulate proliferation within the SVZ? Numerous genes have been shown to control proliferation within this neurogenic niche, including members of the Notch signaling pathway (Imayoshi et al. 2010), *Sox2* (Andreu-Agullo et al. 2012), *Sox9* (Cheng et al. 2009), *Pax6* (Brill et al. 2009), and *Dlx1* and *Dlx2* (Brill et al. 2008). Given previous reports of modulation of Notch pathway signaling by NFI family members (Deneen et al. 2006; Piper et al. 2010), as well as regulation of *Sox9* by NFIX (Heng et al. 2014), it is likely that NFIX can regulate the transcription of at least a subset of these genes, a supposition supported by the presence of putative NFI-binding sites within the promoters of many of the genes implicated within these pathways (Table 5). Thus, NFIX may act to suppress the proliferation of stem cells and transit-amplifying cells within the SVZ during postnatal development. However, another alternative explanation could be that the loss of *Nfix* culminates in a shift in the balance between stem cell quiescence and active cell division.

Table 5 Putative NFI-binding sites within the promoters of genes misregulated in the SVZ of *Nfix*$^{-/-}$ mice

Gene	UCSC identifier	Position relative to TSS	Site *P*-value	Site sequence
Dab1	uc008txv.1	−386	2.8×10^{-5}	GTGGCGGGCTCCCAG
Dab1	uc008txv.1	−489	3.9×10^{-6}	CGGGCGCAGAGCCAA
Dab1	uc008txu.1	−1912	8.2×10^{-5}	TTGGGCAAATGCCAT
Dab1	uc008txv.1	−2618	6.8×10^{-5}	TGGGAAGAGAACCAA
Dlx1	uc008kau.1	−601	1.4×10^{-5}	CTGGCCAGACCCCAG
Dlx1	uc008kau.1	−2946	8.7×10^{-5}	GAGGATCAGGGCCAG
Fscn1	uc009ajl.1	−304	8.4×10^{-6}	TTGGAGATCAGCCAA
Fscn1	uc009ajl.1	−814	8.2×10^{-5}	ATGGCACAGCCCCAA
Fscn1	uc009ajl.1	−1003	1.7×10^{-5}	CTGGGGTAGGGCCAG
Fscn1	uc009ajl.1	−1033	1.1×10^{-5}	AGGGCCAGGGGCCCA
Gdnf	uc007vee.1	44	4.3×10^{-5}	GTGGCCCGAATCCCA
Gdnf	uc007vee.1	−5	9.8×10^{-5}	CTGGGCGGGGCCCCG
Pax6	uc008lla.1	−242	2.1×10^{-5}	CTGGTGCAGAGCCAG
Pax6	uc008lla.1	−716	5.3×10^{-5}	CTGGGAAGAAGACAG
Pax6	uc008lky.1	−937	2.1×10^{-5}	AGGGATGAGAGCCAG
Pax6	uc008lla.1	−1069	6.4×10^{-5}	CTGGCGCGAGGCCCC
Pax6	uc008lku.1	−1095	4.3×10^{-6}	CTGGGAGACAGCCAG
Pax6	uc008lku.1	−1454	1.8×10^{-5}	TTGGATAGGTCCCAA
Pax6	uc008lku.1	−1771	7.7×10^{-5}	GAGGCCCAGGGCCCA
Pax6	uc008llc.1	−2861	6.8×10^{-5}	GTGGGAAGGCTCCAG
Plxnd1	uc009djn.1	102	6.0×10^{-5}	CGGGGGGGGGGCCCG
Plxnd1	uc009djn.1	−162	1.7×10^{-6}	CTGGCCAGGAACCAG
Plxnd1	uc009djn.1	−488	6.0×10^{-5}	GGGGACTGTGGCCAG
Plxnd1	uc009djn.1	−1281	4.6×10^{-5}	AGGGCTCAGAGCCCA
Plxnd1	uc009djn.1	−1311	1.9×10^{-5}	TGGGGTGGGGGCCAG
Plxnd1	uc009djn.1	−2738	7.3×10^{-5}	CTGGACAGTGGCCAT
Sox2	uc008oxu.1	−2065	8.7×10^{-5}	AGGGAAGGCGGCCAC
Sox2	uc008oxu.1	−2411	9.8×10^{-5}	GTGGCGCGCGGACAA
Unc5b	uc007ffe.1	−95	9.8×10^{-5}	CGGGGGCGGAGCCAC
Unc5b	uc007ffd.1	−217	6.8×10^{-5}	GTGGAAAGTGGCCCA
Unc5b	uc007ffd.1	−1613	4.6×10^{-5}	GAGGCGCAGGGCCAG
Unc5b	uc007ffe.1	−2324	3.3×10^{-5}	TGGGAAAGGAGACAG
Unc5b	uc007ffd.1	−2743	4.9×10^{-5}	CAGGAAAGAGGCCCA

Note: All potential NFI-binding sites with *P*-values $\leq 10^{-4}$ were reported in the region of −3000 to +200 bp relative to the TSS of the selected genes.

Within the adult SVZ, neural progenitor cells predominantly exist in a quiescent state, dividing rarely to ensure that the progenitor pool does not become depleted. How stem cell quiescence is maintained remains unclear, although neural activity has been implicated in the regulation of this process within the adult dentate gyrus (Song et al. 2012). Intriguingly, NFIX has recently been shown to contribute to the regulation of quiescence in neural stem cells in vitro (Martynoga et al. 2013). Could the enlarged SVZ in *Nfix*$^{-/-}$ mice reflect a diminution of the quiescent progenitor cell pool and an increase in the dividing pool in these mutants? Given that we begin to see a thickened SVZ at P2, well before the mature SVZ neurogenic niche becomes established, it seems unlikely that aberrant exit from quiescence underlies the phenotype observed here.

In addition to regulating the proliferation of neural progenitor cells, NFIX has also been implicated in the regulation of post-mitotic cell migration within the hippocampus (Heng et al. 2014), cerebellum (Piper et al. 2011) and RMS (this study). The contribution of NFIs to cellular migration within the nervous system has been most extensively investigated with respect to postnatal formation of the cerebellum (Kilpatrick et al. 2010). NFIs, which are expressed by post-mitotic migrating cerebellar granule neurons,

regulate a diverse set of target genes, including *Tag-1*, *ephrin B1*, and *N-cadherin* (Wang et al. 2007, 2010), all of which ensure the efficient migration of newborn granule cells from the germinal external granule layer to the internal granule cell layer.

How could NFIX mediate migration through the nascent RMS to the olfactory bulb? Given the expression of NFIX by both neuroblasts within the adult SVZ and RMS, and by GFAP-positive glia surrounding the RMS, it is likely that factors both intrinsic and extrinsic to migrating neuroblasts are controlled by this transcription factor. There are numerous examples of mouse mutants that exhibit abnormal neuroblast migration, leading to an accumulation of neuroblasts within the SVZ and proximal RMS, and a smaller olfactory bulb. For example, the ablation of cell-autonomous factors within neuroblasts, such as the reelin receptors ApoER2/VLDL, the adaptor protein Dab1 (Andrade et al. 2007), the actin-bundling protein fascin (Sonego et al. 2013) and cyclin-dependent kinase 5 (Hirota et al. 2007), all result in aberrant migration of neuroblasts. Another critical cell-autonomous factor required for neuroblast migration is PSA-NCAM, which facilitates chain migration of neuroblasts through the RMS (Ono et al. 1994; Hu et al. 1996). The reduction in PSA-NCAM expression within the RMS at P20 is indicative of potential regulation of this cell adhesion molecule by NFIX during development. DCX is also important for neuroblast migration within the RMS (Koizumi et al. 2006). We have previously reported numerous potential sites for NFI binding within the promoters of *cyclin-dependent kinase 5*, *Ncam1* and *Dcx* (Plachez et al. 2012), and have also identified potential NFI-binding sites in the proximal promoters of many other of the aforementioned genes (Table 5), a finding that points to NFIX regulating multiple cell-autonomous aspects of neuroblast migration during development.

Our data also indicate that NFIX may regulate neuroblast migration via non-cell-autonomous mechanisms during development. Although neuroblasts begin migrating to the olfactory bulb during late gestation, well before the glial tube develops (Sun et al. 2010), the glial tube has formed by P20, and this structure plays a crucial part in facilitating ongoing neuroblast migration. The dramatic reduction in GFAP-expressing glia within the RMS and olfactory bulb of mutant mice is indicative of delayed glial development, findings supported by the reported roles for NFI family members, including NFIX, in promoting gliogenesis both in vitro (Brun et al. 2009; Singh, Bhardwaj, et al. 2011) and in vivo (Shu et al. 2003; Deneen et al. 2006). Here, we reveal *Gdnf* as a potential direct target for transcriptional activation by NFIX, suggesting a mechanism by which this chemoattractant for neuroblasts (Paratcha et al. 2006) is transcriptionally activated during development. Our array and bioinformatics findings also point to further targets for transcriptional regulation by NFIX in the non-cell-autonomous regulation of neuroblast migration, including *Flt1*, which encodes one of the VEGF receptors. Given the integral role played by the vasculature in supporting and guiding neuroblast migration (Snapyan et al. 2009), these findings provide insights into additional avenues through which NFIX may regulate the development of the RMS.

Taken together, our findings provide a comprehensive insight into how NFIX modulates the development of the postnatal SVZ neurogenic niche, migration within the RMS, as well as the consequences of aberrant formation of these structures with regard to interneuron populations within the olfactory bulb. The diverse genetic programs and identification of further direct transcriptional targets controlled by NFIX within the SVZ and RMS, as well as the role of NFIX expression within mature interneuron populations within the olfactory bulb, remain open questions for future studies.

Supplementary Material

Supplementary material can be found at: http://www.cercor.oxfordjournals.org/

Funding

This work was supported by National Health and Medical Research Council (NHMRC) project grants (grant nos 1003462, 1057751, and 1022308 to M.P. and 569504 to L.J.R.) and by the National Institute of Health and NYSTEM grants (grant nos HL080624, C026714, and C026429 to R.M.G.). The following authors were supported by fellowships: M.P. (Australian Research Council Future Fellowship; FT120100170) and L.J.R. (NHMRC Principal Research Fellowship). Y.H.E.H. was supported by an University of Queensland International Scholarship and L.H. was supported by an Australian Postgraduate Award.

Notes

We thank Chantelle Reid and Erica Little for technical assistance, Prof. Perry Bartlett (Queensland Brain Institute) for provision of the *Dcx*-GFP and *Hes5*-GFP mice, Prof. Pankaj Sah (Queensland Brain Institute) and Prof. Yuchio Yanagawa (Gunma University Graduate School of Medicine, Japan) for provision of the *Gad67*-GFP mice, Rowan Tweedale for critical analysis of the manuscript, and Profs Jane Johnson, Robert Hevner and Ryoichiro Kageyama for kindly providing reagents. *Conflict of Interest*: None declared.

References

Alvarez-Buylla A, Garcia-Verdugo JM. 2002. Neurogenesis in adult subventricular zone. J Neurosci. 22:629–634.

Andrade N, Komnenovic V, Blake SM, Jossin Y, Howell B, Goffinet A, Schneider WJ, Nimpf J. 2007. ApoER2/VLDL receptor and Dab1 in the rostral migratory stream function in postnatal neuronal migration independently of Reelin. Proc Natl Acad Sci USA. 104:8508–8513.

Andreu-Agullo C, Maurin T, Thompson CB, Lai EC. 2012. Ars2 maintains neural stem-cell identity through direct transcriptional activation of Sox2. Nature. 481:195–198.

Bailey TL, Boden M, Buske FA, Frith M, Grant CE, Clementi L, Ren J, Li WW, Noble WS. 2009. MEME SUITE: tools for motif discovery and searching. Nucleic Acids Res. 37:W202–W208.

Bergmann O, Liebl J, Bernard S, Alkass K, Yeung MS, Steier P, Kutschera W, Johnson L, Landen M, Druid H, et al. 2012. The age of olfactory bulb neurons in humans. Neuron. 74:634–639.

Bovetti S, Bovolin P, Perroteau I, Puche AC. 2007. Subventricular zone-derived neuroblast migration to the olfactory bulb is modulated by matrix remodelling. Eur J Neurosci. 25:2021–2033.

Brill MS, Ninkovic J, Winpenny E, Hodge RD, Ozen I, Yang R, Lepier A, Gascon S, Erdelyi F, Szabo G, et al. 2009. Adult generation of glutamatergic olfactory bulb interneurons. Nat Neurosci. 12:1524–1533.

Brill MS, Snapyan M, Wohlfrom H, Ninkovic J, Jawerka M, Mastick GS, Ashery-Padan R, Saghatelyan A, Berninger B, Gotz M. 2008. A dlx2- and pax6-dependent transcriptional code for periglomerular neuron specification in the adult olfactory bulb. J Neurosci. 28:6439–6452.

Brun M, Coles JE, Monckton EA, Glubrecht DD, Bisgrove D, Godbout R. 2009. Nuclear factor I regulates brain fatty acid-

binding protein and glial fibrillary acidic protein gene expression in malignant glioma cell lines. J Mol Biol. 391:282–300.
Campbell CE, Piper M, Plachez C, Yeh YT, Baizer JS, Osinski JM, Litwack ED, Richards LJ, Gronostajski RM. 2008. The transcription factor Nfix is essential for normal brain development. BMC Dev Biol. 8:52.
Cebolla B, Vallejo M. 2006. Nuclear factor-I regulates glial fibrillary acidic protein gene expression in astrocytes differentiated from cortical precursor cells. J Neurochem. 97:1057–1070.
Cheng LC, Pastrana E, Tavazoie M, Doetsch F. 2009. miR-124 regulates adult neurogenesis in the subventricular zone stem cell niche. Nat Neurosci. 12:399–408.
Deneen B, Ho R, Lukaszewicz A, Hochstim CJ, Gronostajski RM, Anderson DJ. 2006. The transcription factor NFIA controls the onset of gliogenesis in the developing spinal cord. Neuron. 52:953–968.
Fujita PA, Rhead B, Zweig AS, Hinrichs AS, Karolchik D, Cline MS, Goldman M, Barber GP, Clawson H, Coelho A, et al. 2011. The UCSC Genome Browser database: update 2011. Nucleic Acids Res. 39:D876–D882.
Gao Z, Ure K, Ables JL, Lagace DC, Nave KA, Goebbels S, Eisch AJ, Hsieh J. 2009. Neurod1 is essential for the survival and maturation of adult-born neurons. Nat Neurosci. 12:1090–1092.
Gleeson JG, Lin PT, Flanagan LA, Walsh CA. 1999. Doublecortin is a microtubule-associated protein and is expressed widely by migrating neurons. Neuron. 23:257–271.
Grant CE, Bailey TL, Noble WS. 2011. FIMO: scanning for occurrences of a given motif. Bioinformatics. 27:1017–1018.
Harris L, Dixon C, Cato K, Heng YH, Kurniawan ND, Ullmann JF, Janke AL, Gronostajski RM, Richards LJ, Burne TH, et al. 2013. Heterozygosity for nuclear factor one X affects hippocampal-dependent behaviour in mice. PloS ONE. 8:e65478.
Harris L, Genovesi LA, Gronostajski RM, Wainwright BJ, Piper M. Forthcoming 2014. Nuclear factor one transcription factors: divergent functions in developmental versus adult stem cell populations. Dev Dynamics; doi:10.1002/dvdy.24182.
Heng YH, Barry G, Richards LJ, Piper M. 2012. Nuclear factor I genes regulate neuronal migration. Neurosignals. 20:159–167.
Heng YH, McLeay RC, Harvey TJ, Smith AG, Barry G, Cato K, Plachez C, Little E, Mason S, Dixon C, et al. 2014. NFIX regulates neural progenitor cell differentiation during hippocampal morphogenesis. Cereb Cortex. 24:261–279.
Hippenmeyer S, Youn YH, Moon HM, Miyamichi K, Zong H, Wynshaw-Boris A, Luo L. 2010. Genetic mosaic dissection of Lis1 and Ndel1 in neuronal migration. Neuron. 68:695–709.
Hirota Y, Ohshima T, Kaneko N, Ikeda M, Iwasato T, Kulkarni AB, Mikoshiba K, Okano H, Sawamoto K. 2007. Cyclin-dependent kinase 5 is required for control of neuroblast migration in the postnatal subventricular zone. J Neurosci. 27:12829–12838.
Holmfeldt P, Pardieck J, Saulsberry AC, Nandakumar SK, Finkelstein D, Gray JT, Persons DA, McKinney-Freeman S. 2013. Nfix is a novel regulator of murine hematopoietic stem and progenitor cell survival. Blood. 122:2987–2996.
Hu H, Tomasiewicz H, Magnuson T, Rutishauser U. 1996. The role of polysialic acid in migration of olfactory bulb interneuron precursors in the subventricular zone. Neuron. 16:735–743.
Imayoshi I, Sakamoto M, Yamaguchi M, Mori K, Kageyama R. 2010. Essential roles of Notch signaling in maintenance of neural stem cells in developing and adult brains. J Neurosci. 30:3489–3498.
Jhaveri DJ, Mackay EW, Hamlin AS, Marathe SV, Nandam LS, Vaidya VA, Bartlett PF. 2010. Norepinephrine directly activates adult hippocampal precursors via beta3-adrenergic receptors. J Neurosci. 30:2795–2806.
Kilpatrick DL, Wang W, Gronostajski R, Litwack ED. 2010. Nuclear factor I and cerebellar granule neuron development: an intrinsic-extrinsic interplay. Cerebellum. 11:41–49.
Kim EJ, Ables JL, Dickel LK, Eisch AJ, Johnson JE. 2011. Ascl1 (Mash1) defines cells with long-term neurogenic potential in subgranular and subventricular zones in adult mouse brain. PloS ONE. 6:e18472.
Koizumi H, Higginbotham H, Poon T, Tanaka T, Brinkman BC, Gleeson JG. 2006. Doublecortin maintains bipolar shape and nuclear translocation during migration in the adult forebrain. Nat Neurosci. 9:779–786.
Kriegstein A, Alvarez-Buylla A. 2009. The glial nature of embryonic and adult neural stem cells. Annu Rev Neurosci. 32:149–184.
Martynoga B, Mateo JL, Zhou B, Andersen J, Achimastou A, Urban N, van den Berg D, Georgopoulou D, Hadjur S, Wittbrodt J, et al. 2013. Epigenomic enhancer annotation reveals a key role for NFIX in neural stem cell quiescence. Genes Dev. 27:1769–1786.
Mason S, Piper M, Gronostajski RM, Richards LJ. 2009. Nuclear factor one transcription factors in CNS development. Mol Neurobiol. 39:10–23.
Merkle FT, Tramontin AD, Garcia-Verdugo JM, Alvarez-Buylla A. 2004. Radial glia give rise to adult neural stem cells in the subventricular zone. Proc Natl Acad Sci USA. 101:17528–17532.
Messina G, Biressi S, Monteverde S, Magli A, Cassano M, Perani L, Roncaglia E, Tagliafico E, Starnes L, Campbell CE, et al. 2010. Nfix regulates fetal-specific transcription in developing skeletal muscle. Cell. 140:554–566.
Murase S, Horwitz AF. 2002. Deleted in colorectal carcinoma and differentially expressed integrins mediate the directional migration of neural precursors in the rostral migratory stream. J Neurosci. 22:3568–3579.
Namihira M, Kohyama J, Semi K, Sanosaka T, Deneen B, Taga T, Nakashima K. 2009. Committed neuronal precursors confer astrocytic potential on residual neural precursor cells. Dev Cell. 16:245–255.
Nguyen-Ba-Charvet KT, Picard-Riera N, Tessier-Lavigne M, Baron-Van Evercooren A, Sotelo C, Chedotal A. 2004. Multiple roles for slits in the control of cell migration in the rostral migratory stream. J Neurosci. 24:1497–1506.
Ono K, Tomasiewicz H, Magnuson T, Rutishauser U. 1994. N-CAM mutation inhibits tangential neuronal migration and is phenocopied by enzymatic removal of polysialic acid. Neuron. 13:595–609.
Paratcha G, Ibanez CF, Ledda F. 2006. GDNF is a chemoattractant factor for neuronal precursor cells in the rostral migratory stream. Mol Cell Neurosci. 31:505–514.
Peretto P, Merighi A, Fasolo A, Bonfanti L. 1997. Glial tubes in the rostral migratory stream of the adult rat. Brain Res Bull. 42:9–21.
Piper M, Barry G, Harvey TJ, McLeay R, Smith AG, Harris L, Mason S, Stringer BW, Day BW, Wray NR, et al. 2014. NFIB-mediated repression of the epigenetic factor Ezh2 regulates cortical development. J Neurosci. 34:2921–2930.
Piper M, Barry G, Hawkins J, Mason S, Lindwall C, Little E, Sarkar A, Smith AG, Moldrich RX, Boyle GM, et al. 2010. NFIA controls telencephalic progenitor cell differentiation through repression of the Notch effector Hes1. J Neurosci. 30:9127–9139.
Piper M, Harris L, Barry G, Heng YH, Plachez C, Gronostajski RM, Richards LJ. 2011. Nuclear factor one X regulates the development of multiple cellular populations in the postnatal cerebellum. J Comp Neurol. 519:3532–3548.

Piper M, Plachez C, Zalucki O, Fothergill T, Goudreau G, Erzurumlu R, Gu C, Richards LJ. 2009. Neuropilin 1-Sema signaling regulates crossing of cingulate pioneering axons during development of the corpus callosum. Cereb Cortex. 19 (Suppl 1):i11–i21.

Pjanic M, Pjanic P, Schmid C, Ambrosini G, Gaussin A, Plasari G, Mazza C, Bucher P, Mermod N. 2011. Nuclear factor I revealed as family of promoter binding transcription activators. BMC Genomics. 12:181.

Plachez C, Cato K, McLeay RC, Heng YH, Bailey TL, Gronostasjki RM, Richards LJ, Puche AC, Piper M. 2012. Expression of nuclear factor one A and -B in the olfactory bulb. J Comp Neurol. 520:3135–3149.

Roybon L, Deierborg T, Brundin P, Li JY. 2009. Involvement of Ngn2, Tbr and NeuroD proteins during postnatal olfactory bulb neurogenesis. Eur J Neurosci. 29:232–243.

Sakamoto M, Imayoshi I, Ohtsuka T, Yamaguchi M, Mori K, Kageyama R. 2011. Continuous neurogenesis in the adult forebrain is required for innate olfactory responses. Proc Natl Acad Sci USA. 108:8479–8484.

Sanai N, Nguyen T, Ihrie RA, Mirzadeh Z, Tsai HH, Wong M, Gupta N, Berger MS, Huang E, Garcia-Verdugo JM, et al. 2011. Corridors of migrating neurons in the human brain and their decline during infancy. Nature. 478:382–386.

Schmid CD, Bucher P. 2010. MER41 repeat sequences contain inducible STAT1 binding sites. PloS ONE. 5:e11425.

Scott CE, Wynn SL, Sesay A, Cruz C, Cheung M, Gomez Gaviro MV, Booth S, Gao B, Cheah KS, Lovell-Badge R, et al. 2010. SOX9 induces and maintains neural stem cells. Nat Neurosci. 13:1181–1189.

Shu T, Butz KG, Plachez C, Gronostajski RM, Richards LJ. 2003. Abnormal development of forebrain midline glia and commissural projections in Nfia knock-out mice. J Neurosci. 23:203–212.

Singh SK, Bhardwaj R, Wilczynska KM, Dumur CI, Kordula T. 2011. A complex of nuclear factor I-X3 and STAT3 regulates astrocyte and glioma migration through the secreted glycoprotein YKL-40. J Biol Chem. 286:39893–39903.

Singh SK, Wilczynska KM, Grzybowski A, Yester J, Osrah B, Bryan L, Wright S, Griswold-Prenner I, Kordula T. 2011. The unique transcriptional activation domain of nuclear factor-I-X3 is critical to specifically induce marker gene expression in astrocytes. J Biol Chem. 286:7315–7326.

Smith CM, Luskin MB. 1998. Cell cycle length of olfactory bulb neuronal progenitors in the rostral migratory stream. Dev Dynamics. 213:220–227.

Snapyan M, Lemasson M, Brill MS, Blais M, Massouh M, Ninkovic J, Gravel C, Berthod F, Gotz M, Barker PA, et al. 2009. Vasculature guides migrating neuronal precursors in the adult mammalian forebrain via brain-derived neurotrophic factor signaling. J Neurosci. 29:4172–4188.

Sonego M, Gajendra S, Parsons M, Ma Y, Hobbs C, Zentar MP, Williams G, Machesky LM, Doherty P, Lalli G. 2013. Fascin regulates the migration of subventricular zone-derived neuroblasts in the postnatal brain. J Neurosci. 33:12171–12185.

Song J, Zhong C, Bonaguidi MA, Sun GJ, Hsu D, Gu Y, Meletis K, Huang ZJ, Ge S, Enikolopov G, et al. 2012. Neuronal circuitry mechanism regulating adult quiescent neural stem-cell fate decision. Nature. 489:150–154.

Sun W, Kim H, Moon Y. 2010. Control of neuronal migration through rostral migration stream in mice. Anat Cell Biol. 43:269–279.

Tamamaki N, Yanagawa Y, Tomioka R, Miyazaki J, Obata K, Kaneko T. 2003. Green fluorescent protein expression and colocalization with calretinin, parvalbumin, and somatostatin in the GAD67-GFP knock-in mouse. J Comp Neurol. 467:60–79.

Walker TL, Yasuda T, Adams DJ, Bartlett PF. 2007. The doublecortin-expressing population in the developing and adult brain contains multipotential precursors in addition to neuronal-lineage cells. J Neurosci. 27:3734–3742.

Wang C, Liu F, Liu YY, Zhao CH, You Y, Wang L, Zhang J, Wei B, Ma T, Zhang Q, et al. 2011. Identification and characterization of neuroblasts in the subventricular zone and rostral migratory stream of the adult human brain. Cell Res. 21:1534–1550.

Wang W, Crandall JE, Litwack ED, Gronostajski RM, Kilpatrick DL. 2010. Targets of the nuclear factor I regulon involved in early and late development of postmitotic cerebellar granule neurons. J Neurosci Res. 88:258–265.

Wang W, Mullikin-Kilpatrick D, Crandall JE, Gronostajski RM, Litwack ED, Kilpatrick DL. 2007. Nuclear factor I coordinates multiple phases of cerebellar granule cell development via regulation of cell adhesion molecules. J Neurosci. 27:6115–6127.

Whitman MC, Greer CA. 2009. Adult neurogenesis and the olfactory system. Prog Neurobiol. 89:162–175.

Young KM, Fogarty M, Kessaris N, Richardson WD. 2007. Subventricular zone stem cells are heterogeneous with respect to their embryonic origins and neurogenic fates in the adult olfactory bulb. J Neurosci. 27:8286–8296.